Abstract

Contents

Chapter 2

Numerical Techniques

In this chapter, I will present the numerical methods relevant to this thesis. The incompressible Navier-Stokes equations describe the time- and spatial-varying velocity field and pressure field. One of the foundations of solving partial differential equations begin with the method of weighted residuals.

2.1 Method of weighted residuals

We discuss the method of weighted residuals which provides a mathematical framework for approximating the solutions of partial differential equations. We first consider a generic linear partial differential equation as,

$$\mathbf{L}[u(x)] = 0, \quad x \in \Omega \tag{2.1}$$

where $\mathbf{L}$ refers to a spatial (linear) differential operator subjected to some boundary conditions within the domain, Ω while $u(x)$ refers to the solution. Typical examples of spatial differential operators are the Laplace, Poisson or Helmholtz operators. In seeking the solution, $u(x)$, we assume that it could be approximated by a finite number of N basis (or expansion) functions, $\Phi(x)$,

$$u(x) \approx u^{\delta}(x) = \sum_{i=0}^{N-1} \hat{u}_i \Phi_i(x), \tag{2.2}$$

where $u^{\delta}(x)$ refers to the approximate solution of $u(x)$, comprising of a linear combination of the product between the i^{th} basis coefficient, $\hat{u}_i$, and a basis function $\Phi_i(x)$, that is defined within Ω. Since $u^{\delta}(x)$ is an approximate solution of equation (2.6), we expect a non-zero difference (or 'error') between the exact solution, $u(x)$, and $u^{\delta}(x)$, known as the residual, R, given as,

$$\mathbf{L}[u^{\delta}(x)] = R[u^{\delta}(x)]. \tag{2.3}$$

The residual depends on the approximate solution $u^{\delta}(x)$, and is non-zero, varying within Ω. In other words, equation (2.6) might not be satisfied everywhere in Ω. We need to place restrictions on the residual, such that it $R \rightarrow 0$, and the approximate solution approaches the exact solution, $u^{\delta}(x) \rightarrow u(x)$. The method of residuals allow us to place a restriction on R is by using N weight (or

test) functions, $v_j(x)$, such that it is orthogonal with the residual,

$$(v_j(x), R[u^\delta(x)]) = 0, \quad j = 0, ..., N-1. \tag{2.4}$$

where $(\,\cdot\,,\,\cdot\,)$ refers to an inner-product, a measure of orthogonality between functions defined as,

$$(f, g) = \int_\Omega f(x)g(x)dx. \tag{2.5}$$

By setting the inner-product to 0, equation (2.4) becomes a system of N ordinary differential equations, where the basis coefficients, $\hat{u}_i$, could be determined as we shall see later. The choice of weight function defines the class of projection methods, and the common projection methods are shown in table 2.1. It is worth noting that the method of weighted residuals describes the projection method, and does not specify the type of basis functions employed. The choice of projection method, and basis expansions will have different solution convergence properties, i.e. how does the residual decay as the number of basis expansions increases? By considering Fourier basis expansions, one can expect exponential convergence, desirable for an efficient representation of turbulent dynamics.

Weight functions	Projection method
$v_j(x) = \delta(x - x_j)$	Collocation
$v_j(x) = \begin{cases} 1 & \text{if } x \in \Omega_j \\ 0 & \text{if } x \notin \Omega_j \end{cases}$	Finite-Volume
$v_j(x) = \phi_j$	Galerkin
$v_j(x) = \frac{\partial R}{\partial \hat{u}_j}$	Least-squares

Table 2.1: Examples of weight functions and projection methods

2.2 Galerkin Projection

The Galerkin projection is a remain as a projection method in finite elements, where the weight functions, $v(x)$, are chosen to be the same as the basis functions, $\Phi(x)$. We will elaborate on what defines being the 'same' later. To demostrate the Galerkin projection method, we consider that the spatial (linear) differential operator in equation (2.1) as a 1D Helmholtz equation,

$$\mathbf{L}[u(x)] \equiv \frac{\partial^2 u(x)}{\partial x^2} - \lambda u(x) - f(x) = 0, \quad x \in \Omega := [0, l] \tag{2.6a}$$

$$u(0) = g_D, \quad \left.\frac{\partial u}{\partial x}\right|_{x=l} = g_N. \tag{2.6b}$$

where λ is a real positive constant, $f(x)$ is the forcing function, and Ω the spatial domain bounded between 0 and l. To ensure that problem is well-posed, we impose both Dirichlet and Neumann

boundary conditions, corresponding to g_D and g_N, at $x = 0$ and $x = l$, respectively. Equation 2.6 is said to be written in the *strong* or *classical* form.

Next, we begin to construct the weak form by taking the inner product of the Helmholtz equation with a weight function, which satisfies the homogeneous Dirichlet boundary conditions by definition, and require this inner product to vanish, that is,

$$(w, \mathbf{L}[u(x)]) = \int_0^l w \left[\frac{\partial^2 u(x)}{\partial x^2} - \lambda u(x) + f(x) \right] \mathrm{d}x = 0. \tag{2.7}$$

This step is equivalent to applying the method of weighted residuals, where $u(x)$ could refer to the approximate solution, $u^\delta(x)$. We perform integration by parts next,

$$\underbrace{\int_0^l \frac{\partial v}{\partial x}\frac{\partial u}{\partial x}\mathrm{d}x + \int_0^l \lambda v u \mathrm{d}x}_{a(v,u)} = \underbrace{\int_0^l v f \mathrm{d}x + \left[v \frac{\partial u}{\partial x} \right]_0^l}_{f(v)}. \tag{2.8}$$

This equation is typically referred to as the weak form of equation (2.6). In compact notation, we define the bilinear and linear forms as,

$$a(v, u) = f(v), \tag{2.9a}$$

where $a(v, u)$ and $f(v)$ are typically refered to as the strain energy and forcing function in structural mechanics, assumed to remain finite. To ensure this, we restrict the choice of solutions $u(x)$ to lie in the functional solution space, $\mathcal{U}$, defined as

$$\mathcal{U} := \{u | u \in H^1, u(0) = g_D\}, \tag{2.10}$$

where $u \in H^1$ contains functions of u in the Sobolev space such that the Dirichlet condition $u(0) = g_D$ is statisfied and the sum of square integral of u and its first derivatives, $\frac{\partial u}{\partial x}$ remains bounded,

$$\int_\Omega \left(u^2 + \left(\frac{\partial u}{\partial x} \right)^2 \right) \mathrm{d}\Omega < \infty. \tag{2.11}$$

We consider functions up to the first-derivatives since the it is the highest-order derivative in equation (2.7). Similarly, the functional space of weight functions, $\mathcal{V}$, is defined as,

$$\mathcal{V} := \{v | v \in H^1, v(0) = 0\}, \tag{2.12}$$

where $v \in H^1$ are functions whose values and first derivatives are square-integrable and satisfy a homogeneous Dirichlet boundary condition at $x = 0$. The generalised weak form is therefore finding $u(x) \in \mathcal{X}$, such that

$$a(v, u) = f(v), \quad \forall v \in \mathcal{W}. \tag{2.13}$$

This formulation is still infinite-dimensional, as the function space $\mathcal{U}, \mathcal{W}$ contain infinitely many

functions. To obtain an approximate solution, $u^\delta(x)$, we restrict ourselves to finite-dimensional subspaces, $\mathcal{U}^\delta \subset \mathcal{U}$, and $\mathcal{V}^\delta \subset \mathcal{V}$. The problem is then to find $u^\delta \in \mathcal{U}^\delta$, such that

$$a(v^\delta, u^\delta) = f(v^\delta), \quad v^\delta \in \mathcal{V}^\delta \tag{2.14}$$

Here, both $u^\delta \in \mathcal{U}^\delta$ and $v^\delta \in \mathcal{V}^\delta$ do not lie in same subspace, necessary for the standard Galerkin projection procedure where they should lie in the same subspace. To overcome this, we lift the solution u^δ into two parts,

$$u^\delta = u^\mathcal{H} + u^\mathcal{D}. \tag{2.15}$$

where $u^\mathcal{H} \in \mathcal{V}^\delta$ satisfies the homogeneous Dirichlet condition, lying in the same subsapce as $w^\delta \in \mathcal{V}^\delta$, and $u^\mathcal{D} \in \mathcal{U}^\delta$ satisfies the Dirichlet boundary conditions $u^\mathcal{D}(0) = g_D$. Substituting this decomposition, the standard Galerkin projection methos is to search for the solution $u^\mathcal{H} \in \mathcal{V}^\delta$ such that,

$$a(v^\delta, u^\mathcal{H}) = f(v^\delta) - a(v^\delta, u^\mathcal{D}). \tag{2.16}$$

We have briefly described the mathematical framework for approximating a solution to the linear (spatial) partial differential operator. In the following, we will expand on the type of basis and weight functions , $\Phi(x)$, specifically, using the spectral/*hp* element method, and describe essential differential and integral operations performed numerically, equation (2.16) reduces to a system of linear equations.

2.3 Spectral/*hp* element methods

The spectral/*hp* element method is a spatial discretisation technique in which the solution domain is partitioned into a set of non-overlapping (finite) elements with size h, each consisting of a linear combination of continuous polynomial functions of up to order P. It leverages the geometric flexibility of classical finite-element methods, allowing for the representation of complex engineering geometries, and the exponential (spectral) convergence properties of classical spectral methods, where the solution error decreases exponentially. Suppose we consider $P+1$ linearly independent polynomials spanning the polynomial space of $\mathcal{P}_P$, the error of a smooth solution with element size of h and polynomial order P has the property of [Karniadakis and Sherwin, 2005],

$$||u(x) - u^\delta(x)|| \leq Ch^P ||u(x)|| \approx \mathcal{O}(h^P). \tag{2.17}$$

where C is some constant. Equation 2.17 implies that the error decreases linearly with h, and exponentially with P.

2.3.1 Domain partition

We consider a one-dimensional domain, Ω defined earlier, and seek to decompose it into a set of N_{el} elements, where Ω^e, refers to the elemental partitions with $1 \geq e \geq N_{el}$ such that they meet at their

boundaries,

$$\Omega = \bigcup_{e=1}^{N_{el}} \Omega^e, \quad \text{where} \bigcap_{e=1}^{N_{el}} \Omega^e = \emptyset \tag{2.18}$$

where e^{th} element is defined as,

$$\Omega^e = \{x | x_{e-1} \geq x \geq x_e\}, \tag{2.19}$$

Each element it then represented by a linear combination, $\phi(x)$, where x is referred to the *global* domain.

2.3.2 Standard Elements

In general, we can expect non-uniform elements so it is useful to define a *standard* element,

$$\Omega_{set} := \{\xi | -1 \geq \xi \geq 1\}, \tag{2.20}$$

where Ω_{st} refers to the standard element, defined over local coordinates, $\xi \in [-1, 1]$. By considering formulations using the standard elements, the formulations of basis expansions, differential and integration operations can be performed in local coordinates, ξ, before mapping the results back to the global domain, x. We can map the standard element into any arbitrary global coordinates based on a linear mapping $\chi^e : \Omega_{st} \to \Omega$,

$$x = \chi^e(\xi) = \frac{1-\xi}{2} x_e + \frac{1+\xi}{2} x_{e+1}, \quad \xi \in \Omega_{st} \tag{2.21}$$

which has an analytical inverse, $(\chi^e)^{-1}(x)$,

$$\xi = (\chi^e)^{-1}(x) = 2\frac{x - x_{e-1}}{x_e - x_{e-1}} - 1, \quad x \in \Omega_{st}. \tag{2.22}$$

In each standard element, we can represent the solution by using a linear combination of local expansion basis, $\phi(\xi)$,

$$\phi_0(\xi) = \frac{1-\xi}{2}, \quad \phi_1(\xi) = (1+\xi)(1-\xi), \quad \phi_2(\xi) = \frac{1+\xi}{2}, \tag{2.23}$$

where ϕ_0, ϕ_2 denotes a linear local expansion basis with $P = 1$, while ϕ_1 is a quadratic local expansion basis with $P = 2$. The approximate solution is now represented as,

$$u^\delta(x) = \sum_{i=0}^{N-1} \hat{u}_i \Phi_i(x) = \sum_{e=0}^{N_{el}-1} \sum_{i=0}^{P} \hat{u}_i^e \phi_i^e(\chi^e(\xi)). \tag{2.24}$$

where $\hat{u}_i^e$, N_{el} refers to the local expansion basis coefficients the number of elements. Consequentially, $u^\delta(x)$ now lie within $\mathcal{X}^\delta$.

$$\mathcal{X}^\delta := \left\{ u^\delta \,\middle|\, u^\delta \in H^1,\ u^\delta(\chi^e(\xi)) \in \text{span}\{\phi_0, \phi_1, \phi_2\},\ e = 1, 2, 3, 4 \right\} \tag{2.25}$$

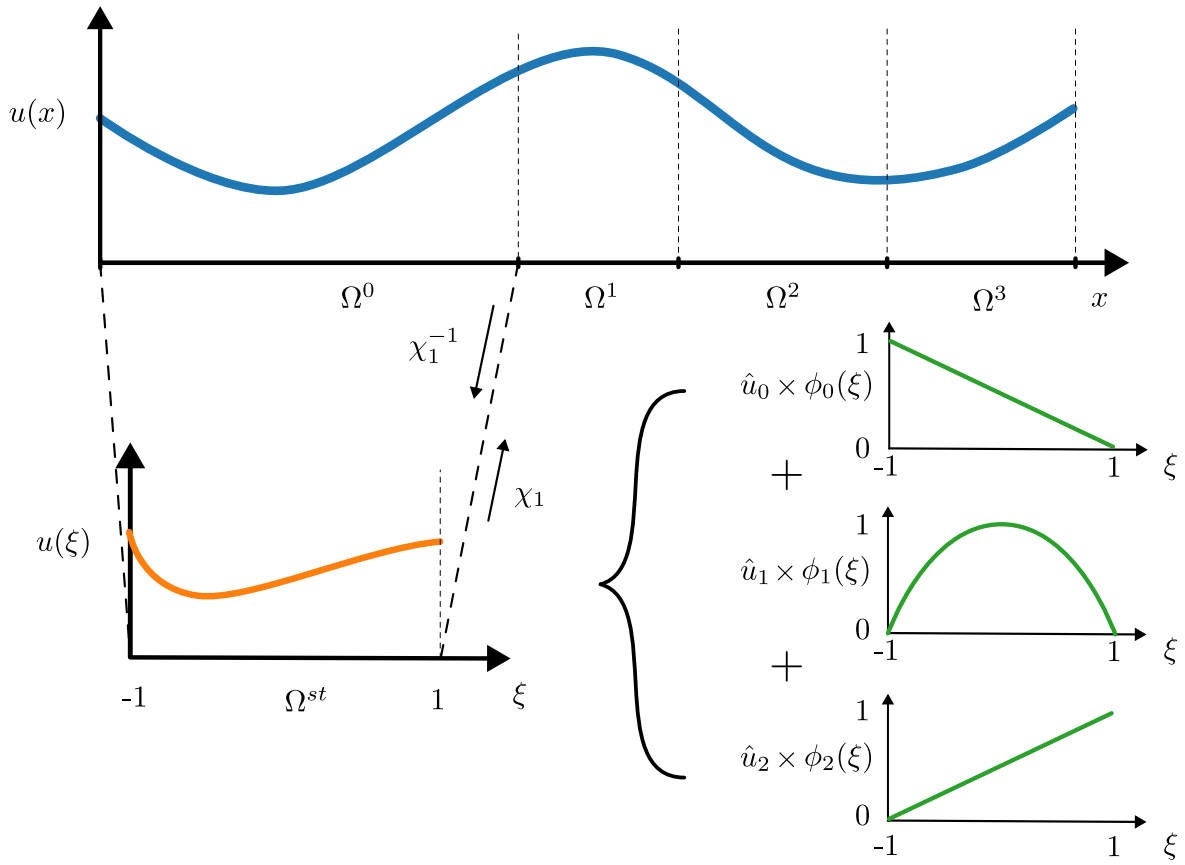

Figure 2.1: A spectral/*hp* element representation of a 1D continuous function, $u(x)$, deomposed into four non-overlapping finite elements, each containing a linear combination of three local expansion bases.

Figure 2.1 summarises the domain partition based on standard elements.

2.3.3 Assembly process

As we represent our solution using local expansion basis within standard elements, their solution across the elemental boundaries may become discontinuous. In the approach of continuous Galerkin projection methods, we enforce our solution to be C^0 continuous across the elemental boundaries. In other words, the neighbouring linear interior elements must meet at the boundaries, such that the local expansion coefficients are constrained by,

$$\hat{u}_P^{e-1} = \hat{u}_0^e. \tag{2.26}$$

This constrain enforeced by consider a mapping between the (global) expansion coefficients, and local expansion coefficients,

$$\hat{\mathbf{u}}_l = \mathbf{A}\hat{\mathbf{u}}_g \tag{2.27a}$$

with,

$$\hat{\mathbf{u}}_l = \begin{bmatrix} \hat{u}_0^1 \\ \hat{u}_1^1 \\ \hat{u}_2^1 \\ \hat{u}_0^2 \\ \hat{u}_1^2 \\ \hat{u}_2^2 \\ \hat{u}_1^3 \\ \hat{u}_2^3 \\ \hat{u}_3^3 \end{bmatrix} \quad \mathbf{A} = \begin{bmatrix} 1 & 0 & 0 & 0 & 0 & 0 & 0 \\ 0 & 1 & 0 & 0 & 0 & 0 & 0 \\ 0 & 0 & 1 & 0 & 0 & 0 & 0 \\ 0 & 0 & 1 & 0 & 0 & 0 & 0 \\ 0 & 0 & 0 & 1 & 0 & 0 & 0 \\ 0 & 0 & 0 & 0 & 1 & 0 & 0 \\ 0 & 0 & 0 & 0 & 1 & 0 & 0 \\ 0 & 0 & 0 & 0 & 0 & 1 & 0 \\ 0 & 0 & 0 & 0 & 0 & 0 & 1 \end{bmatrix}, \quad \hat{\mathbf{u}}_g \begin{bmatrix} \hat{u}_0 \\ \hat{u}_1 \\ \hat{u}_3 \\ \hat{u}_4 \\ \hat{u}_5 \\ \hat{u}_6 \\ \hat{u}_7 \end{bmatrix} \tag{2.27b}$$

where $\hat{\mathbf{u}}_l, \hat{\mathbf{u}}_g, \mathbf{A} \in \mathbb{R}^{N_l, N_g}$ refers to the vector of local, global expansion and scatter matrix, and $N_l = N_{el} \times (P+1)$ refers to the total local degrees of freedom while $N_g = N_l - (N_{el} - 1)$, the global degrees of freedom. Notably, matrix $\mathbf{A}$ 'scatters' the global degrees of freedom to local degrees of freedom. In the spectral/*hp* approach, we typically define local expansion basis, and perform integration and differentiation operation in standard element. After doing so, we need to assemble the operations from the standard element to the global domain by using $\mathbf{A}^T$, is known as an assembly operation, assembling local degrees of freedom to global degrees of freedom. For instance, we wish to perform integration in the domain Ω,

$$\mathbf{I}_g[j] = (\Phi_j(x), u^\delta(x)), \tag{2.28}$$

which equivalent to performing integration using local expansion basis within standard elements, and assembling in the global space by using $\mathbf{A}^T$,

$$\mathbf{I}_g = \mathbf{A}^T \mathbf{I}_l \tag{2.29a}$$

$$\mathbf{I}_g = \begin{bmatrix} \mathbf{I}_0 \\ \vdots \\ \mathbf{I}_{N_g-1} \end{bmatrix}, \quad \mathbf{I}_l = \begin{bmatrix} \mathbf{I}^0 \\ \vdots \\ \mathbf{I}^{N_{el}-1} \end{bmatrix}, \quad \text{where} \quad \mathbf{I}^e = \begin{bmatrix} \int_{-1}^{1} \phi_0^e(\xi) u(\chi^e) \frac{\mathrm{d}\chi^e}{\mathrm{d}\xi} \, \mathrm{d}\xi \\ \vdots \\ \int_{-1}^{1} \phi_{P-1}^e(\xi) u(\chi^e) \frac{\mathrm{d}\chi^e}{\mathrm{d}\xi} \, \mathrm{d}\xi \end{bmatrix} \tag{2.29b}$$

and $\mathbf{I}_g, \mathbf{I}_l, \mathbf{I}^e$ refer to the integration operations perform in global, local and elemental space.

2.3.4 Expansion functions

Here, we discuss the expansion functions of $\phi(\xi)$, where in general could be categorised into *modal* (hierarchical) expansions or *nodal* expansions.

Modal expansions

The most common modal employed in Nektar++ are the Jacobi polynomials, denoted by $P_p^{\alpha,\beta}(x)$, which represent a family of polynomial solutions to the Sturm-Liouville problem wihin, $x \in [-1, 1]$. The Legendre polynomials are a special case of Jacobi polynomials, $L_n(\xi) = P_n^{0,0}(\xi)$ with $\alpha = \beta = 1$. Within the Nektar++ framework, it is common to use the *modified* basis based on Jacobi polynomials, $P_p^{\alpha,\beta}(\xi)$ which are modified with linear elements as

$$\phi_p(\xi) = \psi_p(\xi) = \begin{cases} \frac{1-\xi}{2} & \text{for } p = P \\ \frac{1-\xi}{2}\frac{1+\xi}{2}P_{P-1}^{1,1}(\xi) & \text{for } P \geq 2 \\ \frac{1+\xi}{2} & \text{for } p = P, \end{cases} \tag{2.30}$$

where P denotes the highest polynomial order. Figure 2.2 shows the modified Jacobi polynomials for $p \in [0, 5]$ described by equation 2.30. The boundary modes are ψ_0 and ψ_5 while the rest are boundary modes.

Nodal expansions

A popular nodal expansions are the Lagrange polynomials, common used in the spectral *element* codes such as Semtex and Nek5000. The Lagrange polynomials are given as

$$\phi_p(\xi) = h_p(\xi) = \frac{\prod_{q=0,q\neq p}^{P}(\xi - \xi_q)}{\prod_{q=0,q\neq p}^{P}(\xi_p - \xi_q)} \tag{2.31}$$

The Lagrange polynomials are particular attractive as it has a unit value at ξ_q and zero everywhere else,

$$h_p(\xi_q) = \delta_{pq}. \tag{2.32}$$

Typically, the zeros are located using the zeros of the Gauss-Lobatto polynomials where the zeros are defined using

$$\phi_p(\xi) \to h_p(\xi) = \begin{cases} 1, & \xi = \xi_p, \\ \frac{(\xi^2-1)[P_{Q-1}^{\alpha,\beta}(\xi)]'}{(Q-1)(Q+\alpha+\beta)P_{Q-1}^{\alpha,\beta}(\xi_j)(\xi-\xi_j)}, & \text{otherwise.} \end{cases} \tag{2.33}$$

Figure 2.3 presents nodal expansions based on two-dimensional and one-dimensional Lagrange polynomials, $h_p(\xi_1), h_q(\xi_2)$ respectively.

The modified basis and Lagrange exhibits stark differences.

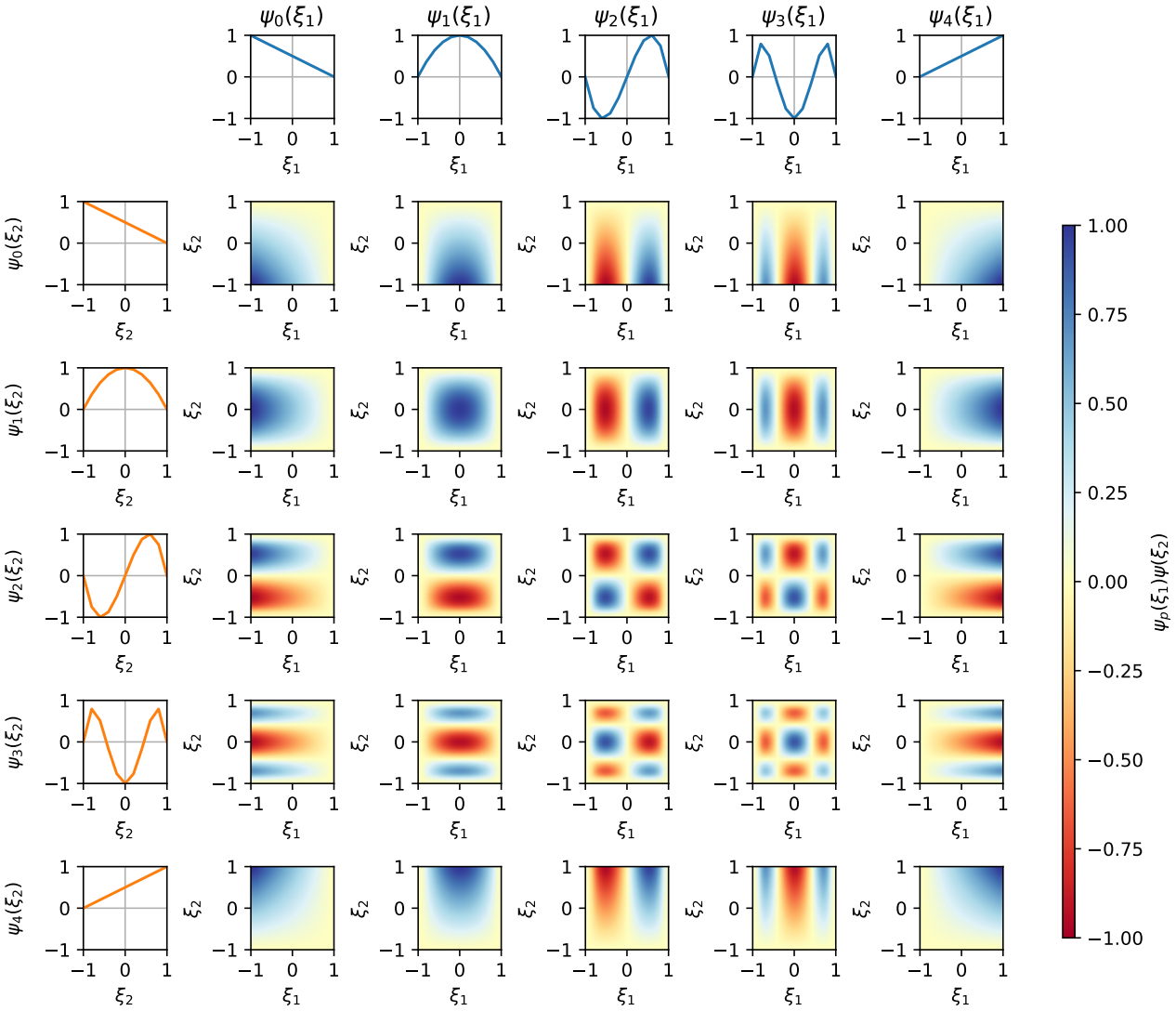

Figure 2.2: Two-dimensional and one-dimension modified basis, $\psi_p(\xi_1)$ and $\psi_q(\xi_2)$, $P = [0, 4]$.

2.3.5 Numerical integration

In the Galerkin formulation, we perform integration routinely. Suppose we want to approximate the integral of a smooth function in a standard element numerically,

$$\int_{-1}^{1} u(\xi)\, \mathrm{d}\xi = \sum_{i=0}^{Q-1} w_i u(\xi_i) + R(u), \tag{2.34}$$

where $Q, w_i, \xi_i, R(u)$ refers to the quadrature points, integration weights and zeros (or abscissae) and the integral of the error. By evaluating the integral, how are we able to minimise the integral error, $R(u)$, with the least number of quadrature points, Q, at some weights and zeros. If $u(\xi)$ is of polynomial order P, we can expect we might need at least $P + 1$ equipspaced points to accurately represent the function and evalute its integral, a rather inefficient method. Gaussain quadrature is allow us to approximate an integral of a function of order P with far lesser thatn $P + 1$ points, as we shall see later. The three generic types of Gaussian quadrature rules are known as: Gauss, Gauss-Radau and Gauss-Lobatto. The main difference between the three methods are in the treatment of the zeros,

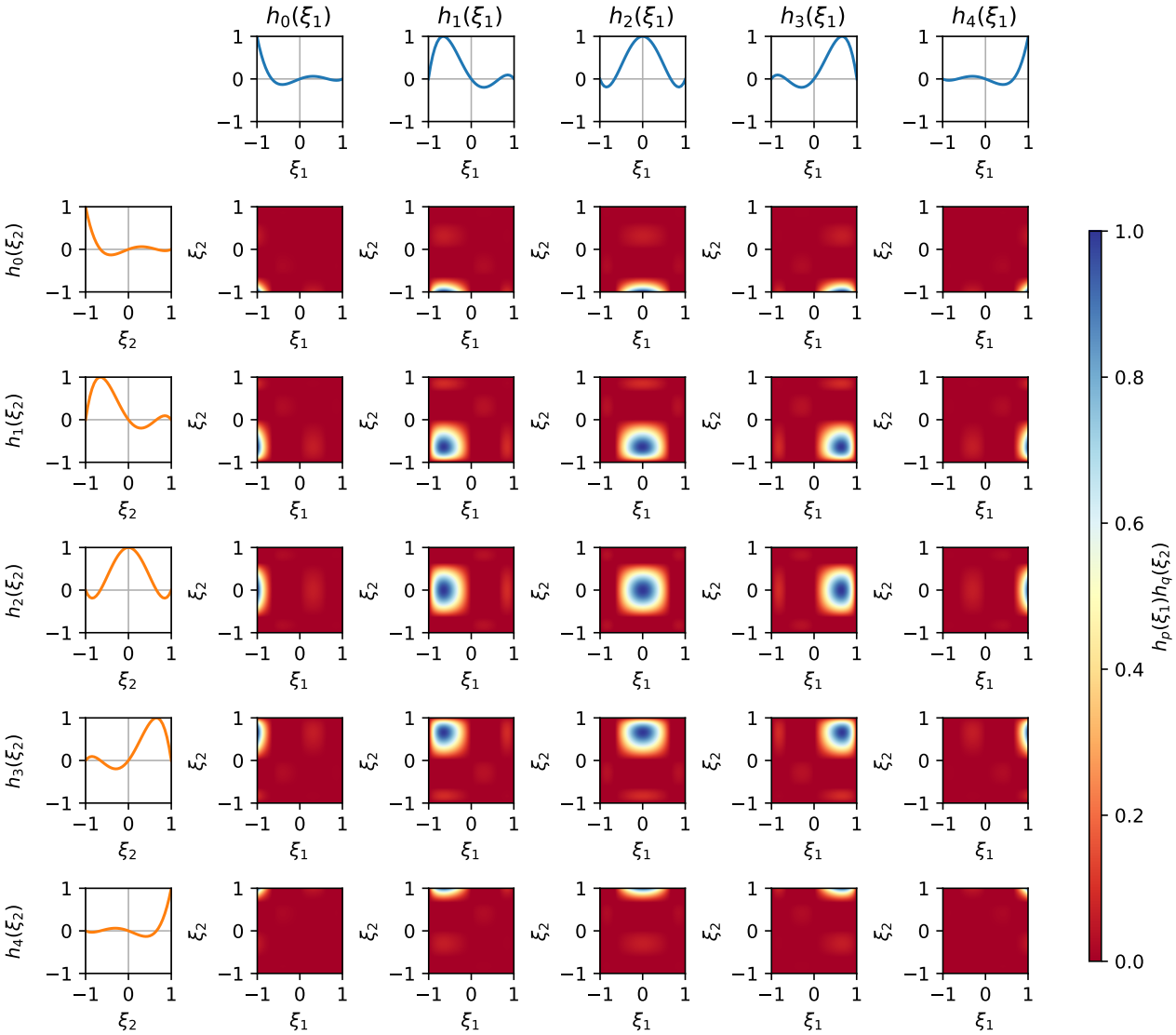

Figure 2.3: Two-dimensional and one-dimension Lagrange basis, $h_p(\xi_1)$ and $h_q(\xi_2)$, $P = [0, 4]$.

where Gauss quadrature uses zeros without the end points $\xi = \pm 1$. Gauss-Radau quadrature either select one of the end points, usually at $\xi = -1$, and Gauss-Lobatto consider the end points. We will only focus on describing the Gauss-Lobatto quadrature rules and the zeros of Jacobi polynomials known as the Gauss-Lobatto-Jacobi quadrature rules given as,

$$\xi_i^{\alpha,\beta} = \begin{cases} -1 & i = 0, \\ \xi_{i-1,Q-2}^{\alpha+1,\beta+1} & i = 1, ..., Q-2, \\ 1, & i = Q-1, \end{cases} \tag{2.35a}$$

$$w_i^{\alpha,\beta} = \begin{cases} (\beta+1)C_{0,Q-2}^{\alpha,\beta}, & i = 0, \\ C_{i,Q-2}^{\alpha,\beta}, & i = 1, ..., Q-2, \\ (\alpha+1)C_{Q-1,Q-2}^{\alpha,\beta}, & i = Q-1, \end{cases} \tag{2.35b}$$

$$C_{i,Q-2}^{\alpha,\beta} = \frac{2^{\alpha+\beta+1}\Gamma(\alpha+Q)\Gamma(\beta+Q)}{(Q-1)(Q-1)!\Gamma(\alpha+\beta+Q+1)[P_{Q-1}^{\alpha,\beta}(\xi_i)]^2} \tag{2.35c}$$

where $w_i^{\alpha,\beta}, \xi_i^{\alpha,\beta}$ are the zeros and weights of the Gauss-Lobatto-Jacobi quadrature rules, and Γ refers to the Gamma function. By using these conventions, we can obtain an exact integral of a continuous function, $u(\xi)$ of polynomial P, with at least $Q \geq (P+3)/2$ quadrature points.

2.3.6 Numerical differentiation

In the same fashion as Gaussian quadrature, we want to numerical differentiate efficiently, a crucial step in the weak formulation of the Helmholtz equations. Suppose that we want to differentiate in x using local coordinates given as,

$$\frac{\mathrm{d}u^\delta(\xi)}{\mathrm{d}x} = \frac{\mathrm{d}u^\delta(\xi)}{\mathrm{d}\xi}\frac{\mathrm{d}\xi}{\mathrm{d}x} = \sum_{p=0}^{P} \hat{u}_p \frac{\mathrm{d}\phi_p(\xi)}{\mathrm{d}\xi}\frac{\mathrm{d}\xi}{\mathrm{d}x}, \tag{2.36}$$

where $\mathrm{d}\xi/\mathrm{d}x$ is simply the Jacobian and the main step in differentiation is in evaluting $\mathrm{d}\phi_p(\xi)/\mathrm{d}\xi$. Now suppose that we express the solution of polynomial order P with Lagrange polynomials, the derivative of the solution commutes,

$$\frac{\mathrm{d}u(\xi)}{\mathrm{d}\xi} = \sum_{i=0}^{Q-1} u(\xi_i)\frac{\mathrm{d}}{\mathrm{d}\xi}h_i(\xi), \tag{2.37}$$

where we only require the derivative to be evaluted at the nodal points, resulting in a derivative matrix of,

$$D_{ij} = \frac{\mathrm{d}h_j(\xi)}{\mathrm{d}\xi}\Big|_{\xi=\xi_i}, \tag{2.38}$$

and the derivative of $u(\xi)$ is simply,

$$\frac{\mathrm{d}u(\xi)}{\mathrm{d}\xi}\Big|_{\xi=\xi_i} = \sum_{j=0}^{Q-1} D_{ij}\hat{u}_j. \tag{2.39}$$

A general representation of the differential operator can be presented as

$$D_{ij} = \begin{cases} \frac{p'_Q(\xi_i)}{p'_Q(\xi_j)}\frac{1}{\xi_i-\xi_j}, & i \neq j, \\ \frac{p''_Q(\xi_i)}{2p'_Q(\xi_i)}, & i = j. \end{cases} \tag{2.40}$$

where $p'_Q(\xi), p''_Q(\xi)$ are specific restricted to the quadrature used. For the Gauss-Lobatto-Jacobi quadrature rules used here, these forms could be found in Appendix C.2 in Karniadakis and Sherwin [2005].

2.3.7 Example in 1D

We have outlined the basic formulation of spectral/*hp* element methods in $1D$ and we will describe its solution procedure, where we start from the weak-form of the Helmholtz equation and convert it into a system of linear equations, amenable to be solved with standard numerical linear algebra techniques. We describe the solution steps as follows,

1. Performing numerical differentiation and integration in the standard region

$$\lambda \underbrace{\int_{-1}^{1} v^{\delta} u^{\mathcal{H}} \, \mathrm{d}\xi}_{\mathbf{M}^e \hat{\mathbf{u}}^e} + \underbrace{\int_{-1}^{1} \frac{\partial v^{\delta}}{\partial \xi} \frac{\partial u^{\mathcal{H}}}{\partial \xi} \mathrm{d}\xi}_{\mathbf{L}^e \hat{\mathbf{u}}^e} = \underbrace{\int_{-1}^{1} v^{\delta} f \mathrm{d}\xi}_{\hat{\mathbf{f}}^e} \tag{2.41}$$

Elemental mass operator

Here we introduce the elemental mass operator given as $\mathbf{M}^e$,

$$\begin{aligned} \int_{-1}^{1} \sum_{i=0}^{P} \hat{v}_i^e \phi_i^e(\xi) \sum_{i=0}^{P} \hat{u}_i^e \phi_i^e(\xi) \, \mathrm{d}\xi &= \sum_{q=0}^{Q} \left[\sum_{i=0}^{P} \hat{v}_i^e \phi_i^e(\xi_q) \sum_{i=0}^{P} \hat{u}_i^e \phi_i^e(\xi_q) \right] w_q^e \\ &= (\hat{\mathbf{v}}^e)^T (\mathbf{B}^e)^T \mathbf{W}^e \mathbf{B}^e \hat{\mathbf{u}}^e \\ &= \hat{\mathbf{v}}^T \mathbf{M}^e \hat{\mathbf{u}}^e \end{aligned} \tag{2.42}$$

where $\mathbf{M}^e = (\mathbf{B}^e)^T \mathbf{W} \mathbf{B}^e$ refers to the elementral mass matrix, while $\mathbf{B}^e \in \mathbb{R}^{Q-1,P}$ and $\mathbf{W}^e \in \mathbb{R}^{Q-1,Q-1}$ refers to the elemental basis and weight matrices, a diagonal matrix consisting of integration weights, w_q^e, respectively,

$$\mathbf{B}^e = \begin{bmatrix} \phi_0(\xi_0) & \cdots & \phi_P(\xi_0) \\ \vdots & \ddots & \vdots \\ \phi_0(\xi_Q) & \cdots & \phi_P(\xi_Q) \end{bmatrix}, \quad \mathbf{W}^e = \begin{bmatrix} w_0^e & & 0 \\ & \ddots & \\ 0 & & w_Q^e \end{bmatrix} \tag{2.43}$$

Elemental laplacian matrices

Now we consider, convert the product of two first-derivatives in to matrix form,

$$\begin{aligned} \int_{-1}^{1} \sum_{i=0}^{P} \hat{v}_i^e \frac{\mathrm{d}\phi_i^e}{\mathrm{d}\xi} \sum_{i=0}^{P} \hat{u}_i^e \frac{\mathrm{d}\phi_i^e}{\mathrm{d}\xi} \, \mathrm{d}\xi &= \sum_{q=0}^{Q} \left[\sum_{i=0}^{P} \hat{v}_i^e D_{qi}^e \phi_i^e(\xi_q) \sum_{i=0}^{P} \hat{u}_i^e D_{qi}^e \phi_i^e(\xi_q) \right] w_q^e \\ &= \hat{\mathbf{v}}^T (\mathbf{B}^e)^T (\mathbf{D}^e)^T \mathbf{W}^e \mathbf{D}^e \mathbf{B}^e \hat{\mathbf{u}}^e \\ &= \hat{\mathbf{v}}^T \mathbf{L}^e \hat{\mathbf{u}}^e \end{aligned} \tag{2.44}$$

where $\mathbf{L}^e = (\mathbf{B}^e)^T (\mathbf{D}^e)^T \mathbf{W} \mathbf{D}^e \mathbf{B}^e$ refers to the elementral Laplacian matrix.

Forcing vector

Lastly, we consider the right-hand side,

$$\begin{aligned}\int_{-1}^{1}\sum_{i=0}^{P}\hat{v}_i^e\phi_i^e(\xi)f^e(\xi)\,\mathrm{d}\xi &= \sum_{q=0}^{P}\sum_{i=0}^{P}\hat{v}_i^e\phi_i^e(\xi_q)f^e(\xi_q)w_q^e, \\ &= \hat{\mathbf{v}}^T(\mathbf{B}^e)^T\mathbf{W}^e\mathbf{f}^e \\ &= \hat{\mathbf{v}}^T\hat{\mathbf{f}}^e,\end{aligned} \tag{2.45}$$

where $\hat{\mathbf{f}}^e$, is referred to the elemental forcing vector. As we consider all of the matrices, the Helmholtz equations in elemental form is simply solving for,

$$\left[\lambda\mathbf{M}^e+\mathbf{L}^e\right]\hat{\mathbf{u}}^e=\hat{\mathbf{f}}^e. \tag{2.46}$$

If we considered bolting the elements together and the boundary conditions,

$$\lambda\underbrace{\begin{bmatrix}\mathbf{M}^0+\mathbf{L}^0 & & \mathbf{0}\\ & \ddots & \\ \mathbf{0} & & \mathbf{M}^{N_{el}-1}+\mathbf{L}^{N_{el}-1}\end{bmatrix}}_{\mathbf{M}_l+\mathbf{L}_l}\underbrace{\begin{bmatrix}\hat{\mathbf{u}}^0\\ \vdots\\ \hat{\mathbf{u}}^{N_{el}-1}\end{bmatrix}}_{\hat{\mathbf{u}}_l}=\underbrace{\begin{bmatrix}\hat{\mathbf{f}}^0\\ \vdots\\ \hat{\mathbf{f}}^{N_{el}-1}\end{bmatrix}}_{\hat{\mathbf{f}}_l}+\underbrace{\begin{bmatrix}\mathbf{L}^0g_D\\ \vdots\\ \mathbf{0}\end{bmatrix}}_{\mathbf{g}_D}+\underbrace{\begin{bmatrix}\mathbf{0}\\ \vdots\\ g_N\end{bmatrix}}_{\mathbf{g}_N}, \tag{2.47}$$

where $\mathbf{M}_l, \mathbf{L}_l, \hat{\mathbf{u}}_l, \hat{\mathbf{f}}_l, \mathbf{g}_D, \mathbf{g}_N$ refers to the local mass matrix, local laplacian matrix, and vector of local expansion coefficients , Dirichlet and Neumann boundary conditions. Finally, we can assemble them using the assembly matrix,

$$\mathbf{A}^T(\lambda\mathbf{M}_l+\mathbf{L}_l)\mathbf{A}\hat{\mathbf{u}}_g=\mathbf{A}^T(\hat{\mathbf{f}}^l+\mathbf{g}_D+\mathbf{g}_N), \tag{2.48}$$

2.4 Numerical techniques for solving the Navier-Stokes equations

2.4.1 Velocity Correction Scheme

While methods for temporal and spatial discretisation have been discussed, it is not possible to apply these techniques in a straight-forward manner to the incompressible Navier-Stokes equations. This is because of the unique role of the pressure field which ensures that the time-dependent velocity field is divergence-free. However, the velocity and the pressure fields form a coupled-system through the continuity and momentum equations which requires the solution of both fields simultaneously. In general, there are 3 ways to deal with velocity-pressure coupling: (1) Coupled methods (*Uzawa* method), (2) Change of variables (streamfunction-vorticity formulation) and (3) Splitting methods which decouples velocity and pressure. The velocity correction scheme (VCS) (**?**), a type of splitting method, decouples the velocity field from the pressure field used in *nektar++* will be discussed in this section. The velocity correction scheme is a stiffly-stable time-integration (IMEX) scheme which

treats the nonlinear terms (advection) explicitly and linear terms (pressure gradient and diffusion) implicitly. The VCS will be demonstrated through a worked example. The incompressible Navier-Stokes equations with unit density, constant density and viscosity is written as,

$$\frac{\partial \mathbf{u}}{\partial t} = \mathbf{N}(\mathbf{u}) - \nabla p + \nu \mathbf{L}(\mathbf{u}), \qquad \nabla \cdot \mathbf{u}, \tag{2.49}$$

where $\mathbf{u},\ p,\ \rho,\ \nu$ refers to the fluid's velocity, pressure, density and kinematic viscosity respectively. The convection and diffusion terms are conveniently written as nonlinear and linear functions,

$$\mathbf{N}(\mathbf{u}) \equiv -(\mathbf{u} \cdot \nabla)\mathbf{u} = -\frac{1}{2}\left[(\mathbf{u} \cdot \nabla)\mathbf{u} + \nabla \cdot (\mathbf{u}\mathbf{u})\right], \qquad \mathbf{L}(\mathbf{u}) \equiv \nabla^2 \mathbf{u}. \tag{2.50}$$

The nonlinear terms are written in the skew-symmetric to minimise aliasing errors (**?**). The first step in the scheme is to time integrate the nonlinear terms explicitly,

$$\frac{\hat{\mathbf{u}} - \sum_{q=0}^{J_e-1} \alpha_q \mathbf{u}^{n-q}}{\Delta t} = \sum_{q=0}^{J_e-1} \beta_q \mathbf{N}(\mathbf{u}^{n-q}), \tag{2.51}$$

where $\hat{\mathbf{u}}$ is the first intermediate velocity field, J_e denotes the order of the explicit scheme, superscript n denotes the solution at the n^{th} time-step and $\alpha_q,\ \beta_q$ refers to constant related to the IMEX schemes. Next, the second intermediate velocity field $\hat{\hat{\mathbf{u}}}$ is obtained from the gradient of the pressure field at $n+1$,

$$\frac{\hat{\hat{\mathbf{u}}} - \hat{\mathbf{u}}}{\Delta t} = -\nabla p^{n+1}. \tag{2.52}$$

However, the pressure field at time-step $n+1$ is not known. Taking the divergence of equation 2.52, and assuming that $\hat{\hat{\mathbf{u}}}$ is divergence-free, the Poisson equation for pressure is given as,

$$\nabla^2 p^{n+1} = \nabla \cdot \left(\frac{\hat{\mathbf{u}}}{\Delta t}\right). \tag{2.53}$$

with the following boundary condition,

$$\frac{\partial p^{n+1}}{\partial n} = \mathbf{n} \cdot \left(\frac{\hat{\hat{\mathbf{u}}} - \hat{\mathbf{u}}}{\Delta t}\right) \tag{2.54}$$

However, this boundary condition often suffer from splitting errors and may lead to wrong solutions (**?**). To rectify this, the boundary condition is directly obtain by taking normal dot product with 2.49 and evaluated explicity (**?**),

$$\frac{\partial p^{n+1}}{\partial t} = -\sum_{q=0}^{J_e-1} \beta_q \left[\frac{1}{\Delta t}\mathbf{u}^{n-q} + \nu(\nabla \times \omega^{n-q}) + (\mathbf{u}^{n-q} \cdot \nabla)\mathbf{u}^{n-q}\right] \cdot \mathbf{n}. \tag{2.55}$$

where $\omega = \nabla \times \mathbf{u}$, J_e is the order for the explicit scheme, β_q is the coefficient related to the time-integration scheme. We obtain the pressure field at time-step $n+1$ by solving the pressure Poisson equation (2.53) with the modified boundary conditions (2.55). Then, the second intermediate velocity

field $\hat{\hat{\mathbf{u}}}$ is obtained from equation 2.52. Finally, the velocity field at $n+1$ is obtain from the final step of the scheme by solving

$$\frac{\gamma_0 \mathbf{u}^{n+1} - \hat{\hat{\mathbf{u}}}}{\Delta t} = \nu \sum_{q=0}^{J_i-1} \beta_q \mathbf{L}(\mathbf{u}^{n+1-q}), \qquad \mathbf{u}^{n+1}|_{\delta\Omega} = g_D \tag{2.56}$$

where J_i denotes the order of the implicit scheme, γ_0, β_q are coefficients related to the stiffly stable time-integration scheme and $\mathbf{u}^{n+1}$ satisfies the Dirichlet boundary conditions. Table 2.2 shows the coefficients of stiffly-stable time-integration schemes (**?**).

test	1^{st} order	2^{nd} order
γ_0	1	3/2
β_0	1	2
β_1	0	-1
α_0	0	-1/2
α_1	0	0

Table 2.2: Stiffly-stable splitting scheme coefficients

2.4.2 Fourier spectral/*hp* modes

The Fourier spectral/*hp* element method uses a combination of Fourier expansions and spectral/*hp* element method to discretise the spatial domain. In a turbulent channel flow, the Fourier expansions are used to represent the periodic streamwise and cross stream directions, while the spectral/*hp* elements are used to discretise the wall-normal direction. Within the *nektar++* framekwork, the Fourier spectral/*hp* element method (also known as a Quasi-3D approach), can be implemented either with 2D spectral/*hp* elements and 1D Fourier expansions (3DH1D) or 1D spectral/*hp* elements and 2D Fourier expansions (3DH2D). In this work, the 2D spectral/*hp* elements with 1D Fourier expansions are used to discretise the cross stream plane and streamwise flow respectively. The use of 2D spectral/*hp* elements in the cross stream plane is necessary to represent the riblet geometry (**?**). The time- and spatially-varying velocity and pressure in the cross stream planes are approximated as a finite sum of 2D modified Jacobi polynomials up to the P^{th}-order,

$$\begin{bmatrix} \mathbf{u}^{\delta}(y,z,t) \\ p^{\delta}(y,z,t) \end{bmatrix} = \sum_{p=0}^{P} \sum_{q=0}^{P} \psi_p(y)\psi_q(z) \begin{bmatrix} \hat{\mathbf{u}}_{p,q}(t) \\ \hat{p}_{p,q}(t) \end{bmatrix} \tag{2.57}$$

where $\hat{\mathbf{u}}_{p,q}(t)$ and $\hat{p}_{p,q}(t)$ are the time-varying coefficients. Extending equation 2.57 to include the streamwise direction represented by Fourier expansions,

$$\begin{bmatrix} \mathbf{u}^{\delta}(x,y,z,t) \\ p^{\delta}(x,y,z,t) \end{bmatrix} = \sum_{k=0}^{N-1} \sum_{p=0}^{P} \sum_{q=0}^{P} \psi_p(y)\psi_q(z) e^{ik\alpha x} \begin{bmatrix} \hat{\mathbf{u}}_{p,q,k}(t) \\ \hat{p}_{p,q,k}(t) \end{bmatrix} = \sum_{k=0}^{N-1} e^{ik\alpha x} \begin{bmatrix} \mathbf{u}_k(y,z,t) \\ p_k(y,z,t) \end{bmatrix} \tag{2.58}$$

where $\alpha = \frac{2\pi}{L_x}$ is the streamwise wavenumber, L_x is the streamwise domain length and N refers to the number of Fourier expansions. Substituting equation 2.58 into the Navier-Stokes equations and taking the Fourier transform (equivalently to the Galerkin projection with respect to Fourier expansion as a test function) yields N-systems of equations,

$$\frac{\partial \mathbf{u}_k}{\partial t} = -\tilde{\nabla}_k p_k + \nu(\nabla^2_{y,z} - k^2\alpha^2)\mathbf{u}_k - [\widehat{(\mathbf{u}\cdot\nabla)\mathbf{u}}]_k, \qquad \tilde{\nabla}\mathbf{u}_k = 0 \tag{2.59}$$

where, $\tilde{\nabla} = (ik\alpha, \frac{\partial}{\partial y}, \frac{\partial}{\partial z})$, $\nabla^2_{y,z} = (\frac{\partial^2}{\partial y^2}, \frac{\partial^2}{\partial z^2})$ and $[\widehat{(\mathbf{u}\cdot\nabla)\mathbf{u}}]_k$ refers to the Fourier-transformed of the k^{th} nonlinear term.

2.4.3 Enforcing constant flow rate

Due to the enforced periodicity in the streamwise z direction via Fourier expansions, a pressure drop cannot be prescribed to drive the flow for $Re > 0$ scenarios. To sustain the flow, we use a Green's function approach [**?**] to impose a constant flow rate,

$$W_b = Q(\mathbf{u}) = \frac{1}{2L_x h}\int_{x,y} \mathbf{u}\, \mathrm{d}x\mathrm{d}z, \tag{2.60}$$

where W_b and $Q(\cdot)$ refer to the desired flow rate and flow rate operator. A correction velocity, $\mathbf{u}_{corr}$, is obtained by solving the linear Stokes equation with unit forcing once and is stored for reuse. At the end of every time-step, the final velocity field, $\mathbf{u}$, is then updated by adding this correction velocity to the homogeneous velocity obtained from the velocity correction scheme,

$$\mathbf{u} = \mathbf{u}_h + \gamma\mathbf{u}_{corr}, \tag{2.61}$$

where γ defined as,

$$\gamma = \frac{W_b - Q(\mathbf{u}_h)}{Q(\mathbf{u}_{corr})}, \tag{2.62}$$

is adjusted to satisfy the desired flow rate, W_b. The flow rate, W_b, is related to the laminar centreline velocity $W_c = 3/2W_b$, which defines the Reynolds number, $Re = W_c h/\nu$. For more details on the numerical method, the reader is referred to **?**.

2.5 Stability analysis of the Navier-Stokes equations

2.5.1 Linear Stability analysis

2.5.2 Edge state computations

Consider equation 2.60 to be a solution of a 1-dimensional Poisson equation, bounded by the domain $\Omega \in [x_a, x_b]$, Next, we consider that the expansion functions, $\phi_i(x)$, belongs to an element of a Hilbert space, with a suitable inner-product.

The mathematical framework begins by first assuming that the solution, $u(x)$, is an element of a Hilbert space, $\mathcal{H}$ with a suitable inner-product $(\cdot, \cdot)$ and norm $||\cdot||$. For SEMs belong to a general class of methods known as the method of weighted residual, a generic method for approximating a solution of a differential equation. The method of weighted residual will be described with a worked example as follows. Consider that the solution of a differential equation $u(x)$ can be represented as an infinite sum of *trial* [Karniadakis and Sherwin, 2005]. functions (also known as basis functions, expansion functions, mode shapes).

(2.63)

where $\phi_i(x)$ are the *trial* functions and $\hat{u}_i$ are the trial function coefficients to be determined. with the appropriate boundary conditions, and $\mathbb{L}$ refers to a linear differential operator. Note that equation 2.60 exactly satisfies the differential equation of **??** i.e $\mathbb{L}u(x) - f(x) = 0$. The exact solution would require a computation of infinite basis coefficients $\hat{u}$ which is practically infeasible. Therefore, an approximate solution $u^\delta(x)$ is sought after by truncating an infinite number of basis expansions to a finite number,

$$u(x) \approx u^\delta(x) = \sum_{i=0}^{K} \hat{u}_i \phi_i(x), \tag{2.64}$$

where there is a finite number of K basis expansions. The approximate solution does not satisfy **??** exactly, leading to an 'error' known as a residual,

$$R(u^\delta(x)) = \mathbb{L}u^\delta(x) - f(x) \tag{2.65}$$

The method of weighted residual is a general method that allows for various types the restriction to be implemented. The method "nullifies" the residual by equating the inner product with a *test* function, $v_j(x)$ (also known as a weight function - hence the name 'weighted residual') to zero,

$$(v_j(x), R(u^\delta(x))) = \int_{x_a}^{x_b} v_j \, R(u^\delta(x)) \, \mathrm{d}x = 0, \qquad j = 0, ..., K. \tag{2.66}$$

Galerkin methods are commonly found in finite/spectral element solvers, used in *nektar++*. The Galerkin method belongs to a general class of weighted residual methods that assumes the *trial* functions take on the same form as the *test* functions (Table 2.1). To describe the method, a worked example is illustrated. The Galerkin method is appplied to solve the Poisson equation **??** with the following boundary conditions,

$$B^- = g^- \quad \text{at} \quad x = x_a, \qquad B^+ = g^+ \quad \text{at} \quad x = x_b \tag{2.67}$$

where B^-, B^+ are the boundary conditions which could be either Dirichlet, Neumann or Robin conditions. Equation **??** and 2.64 together forms a boundary value problem and is said to be in the *strong* [1] form. The Galerkin method assumes that the trial functions $\phi_i(x)$ satisfies equation **??** with

[1] *strong* loosely mean that the trial functions are required to be both C^0 and C^1 continuous

homogeneous boundary conditions,

$$\phi_i(x_a) = \phi_i(x_b) = 0. \tag{2.68}$$

Next, the solution $u(x)$ is decomposed into a linear combination of $\tilde{u}(x)$ and $u^H(x)$,

$$u(x) = \tilde{u}(x) + u^H(x), \tag{2.69}$$

where $\tilde{u}(x)$ is any function that satisfy the boundary conditions assosciated with equation 2.64 and $u^H(x)$ is the homogeneous solution that satisfies the homogeneous boundary conditions - $B_H^-(x_a) = B_H^+(x_b) = 0$. The resulting problem for $u^H(x)$ becomes

$$\mathbb{L}u^H(x) - h(x) = 0, \qquad x_a \leq x \leq x_b, \tag{2.70}$$

where $h = f(x) - \mathbb{L}\tilde{u}(x)$. It is worth noting that the steps thus simply mathematical, and no approximation have been made. The solutions of $u(x) = \tilde{u}(x) - u^H(x)$ represented by an infinite expansions (equation 2.60) are exact. Next, the homogeneous solution $u^H(x)$ can be approximated by a finite expansion of *trial* functions,

$$u^H(x) \approx u^{H,\delta}(x) = \sum_{i=0}^{K} \hat{u}_i^{H,\delta} \phi_i(x), \tag{2.71}$$

where $\hat{u}_i^{H,\delta}$ are the coefficients to be determined. Since $\phi_i(x)$ satisfies the homogeneous boundary conditions, $\hat{u}_i^{H,\delta}$ can take on any values and $u^{H,\delta}(x)$ will still satisfy the homogeneous boundary conditions. Substituing the approximate solution of $u^{H,\delta}(x)$ into equation 2.67, and applying the method of weighted resiudal,

$$(R(u^{H,\delta}), v_j(x)) = \int_{x_a}^{x_b} \left(\mathbb{L}u^{H,\delta}(x) - h(x)\right) v_j(x)\, \mathrm{d}x = 0, \qquad j = 0, ..., K, \tag{2.72}$$

where $v_j(x)$ is some *test* function and there are $K+1$ finite expansions. In the Galerkin method (or Bubnov-Galerkin), the weight function $v_j(x)$ takes on the same form as the trial functions $\phi_j(x)$ (Table 2.1). In other words, the differential equation is satisfied when projected on the *test/trial* functions. Substituting equation 2.68 into the residual equation 2.69 and applying $v_j(x) = \phi_j(x)$,

$$\sum_{i=0}^{K} \hat{u}_i^{H,\delta} \int_{x_a}^{x_b} \mathbb{L}\phi_i \phi_j \, \mathrm{d}x = \int_{x_a}^{x_b} \left(f(x) - \mathbb{L}\tilde{u}(x)\right) \phi_j \, \mathrm{d}x, \qquad j = 0, .., K \tag{2.73}$$

Equation 2.70 furnishes a system of $K+1$ linear equations with $K+1$ unknowns i.e $\{\hat{u}_0^{H,\delta}, ..., \hat{u}_K^{H,\delta}\}$. Applying integration by parts to equation 2.70, the equation reduces to,

$$\sum_{i=0}^{K} \hat{u}_i^{H,\delta} \left[\int_{x_a}^{x_b} \frac{\partial \phi_j}{\partial x}\frac{\partial \phi_i}{\partial x} + \lambda \phi_j \phi_i \, \mathrm{d}x\right] = -\int_{x_a}^{x_b} \frac{\partial \tilde{u}}{\partial x}\frac{\partial \phi_j}{\partial x} + (\lambda \tilde{u} + f(x))\phi_j \, \mathrm{d}x, \tag{2.74}$$

which is known as the *weak*[2] form. The boundary conditions of the *weak* form naturally appears in the right-hand side of equation 2.72, which makes it convenient to implement. Equation 2.70 can be re-written in matrix form,

$$\begin{bmatrix} \int_{x_a}^{x_b} \frac{\partial \phi_0}{\partial x}\frac{\partial \phi_0}{\partial x} + \lambda\phi_0\phi_0 \, \mathrm{d}x & \dots & \int_{x_a}^{x_b} \frac{\partial \phi_0}{\partial x}\frac{\partial \phi_K}{\partial x} + \lambda\phi_0\phi_K \, \mathrm{d}x \\ \vdots & \ddots & \vdots \\ \int_{x_a}^{x_b} \frac{\partial \phi_K}{\partial x}\frac{\partial \phi_0}{\partial x} + \lambda\phi_0\phi_0 \, \mathrm{d}x & \dots & \int_{x_a}^{x_b} \frac{\partial \phi_K}{\partial x}\frac{\partial \phi_K}{\partial x} + \lambda\phi_0\phi_K \, \mathrm{d}x \end{bmatrix} \begin{bmatrix} \hat{u}_0^{H,\delta} \\ \vdots \\ \hat{u}_K^{H,\delta} \end{bmatrix} = \begin{bmatrix} -\int_{x_a}^{x_b} \frac{\partial \tilde{u}}{\partial x}\frac{\partial \phi_0}{\partial x} + (\lambda\tilde{u} + f(x))\phi_0 \, \mathrm{d}x \\ \vdots \\ -\int_{x_a}^{x_b} \frac{\partial \tilde{u}}{\partial x}\frac{\partial \phi_K}{\partial x} + (\lambda\tilde{u} + f(x))\phi_K \, \mathrm{d}x \end{bmatrix} \tag{2.75}$$

where $\hat{\mathbf{u}}^{H,\delta} = [\hat{u}_0^{H,\delta}, ..., \hat{u}_K^{H,\delta}]$ is determined by solving the system of linear equations.

2.6 The Spectral/hp element methods

To represent the spatially-dependent velocity and pressure fields, spatial discretisation is performed using the spectral/*hp* element method. Other popular methods of spatial discretisation found in literature are the finite-difference methods, and finite-volume methods. The spectral/hp element method (SEM) is related to the Galerkin method in which the type of *trial* function used. The spectral/*hp* element method combines 2 traditional numerical methods, namely,

1. Finite elements:

   The finite element method decomposes the global domain into a set of non-overlapping subdomains (finite elements), represented by linear shape functions. In a 1D domain, the size of each element is given by h and the approximate solution should covergence as h is decreased - also known as *h*-refinement. The flexibility of domain decomposition allows for complex engineering geometries to be represented.

2. Spectral method:

   The spectral method performs a global discretisation of the domain. The domain is represented by a linear combination of global continuous functions, such as the Fourier series. Spectral methods benefit from the property of *spectral convergence*, where the solution error decreases by $\mathcal{O}(c^{-N})$, where c is some constant $0 \leq c \leq 1$ and N is the number of polynomials (**?**). In other words, as the number of functions is increased, the error decreases exponentially.

The Spectral/*hp* element method leverages the advantages of both methods - geometric flexibility and spectral covergence. The spectral/*hp* method uses a series of high-order polynomials (Lagrange/Legendre) within each element. Considering each element consists of $P + 1$ linearly independent polynomials (where P refers to the highest polynomial order) spanning the polynomial

[2] *trial* functions are only required to be C^0 continuous

space of $\mathcal{P}_P$, the error of a smooth solution with mesh-size h and polynomial order P has the property of (**?**),

$$||u(x) - u^{\delta}(x)|| \leq Ch^{P}||u(x)|| \approx \mathcal{O}(h^{P}). \tag{2.76}$$

Equation 2.73 implies that the error decreases as the h is decrease (mesh refinement) or as P is increased using higher-order polynomials.

2.7 Velocity correction scheme for incompressible Navier Stokes equations

2.8 Linear Stability Analysis

2.9 Edge Tracking

To study the dynamics of infinitetisimal perturbations about a base flow, the time evolution equation for the perturbations dynamics typically reduces to,

$$\frac{\partial}{\partial t}\mathbf{u} = \mathcal{L}\mathbf{u}, \tag{2.77}$$

where $\mathcal{L}, \mathbf{u}$ refers to the linearised operator and a vector of perturbations. Suppose the that linear operator is diagonlisable,

$$\mathcal{L} = \begin{bmatrix} | & & | \\ \mathbf{s}_1 & \cdots & \mathbf{s}_n \\ | & & | \end{bmatrix} \begin{bmatrix} \lambda_1 & & 0 \\ & \ddots & \\ 0 & & \lambda_n \end{bmatrix} \begin{bmatrix} | & & | \\ \mathbf{s}_1 & \cdots & \mathbf{s}_n \\ | & & | \end{bmatrix}^{-1} = \mathcal{S}\Lambda\mathcal{S}^{-1}. \tag{2.78}$$

Suppose we can decompose our initial conditions into a superposition of eigenmodes,

$$\mathbf{u}_0 = \alpha_{1,0}\mathbf{s}_1 + \alpha_{2,0}\mathbf{s}_2 + ... + \alpha_{N,0}\mathbf{s}_n = \sum_{i=1}^{n} \alpha_{i,0}\mathbf{s}_i, \tag{2.79}$$

and w

Edge state tracking

Computing Invariant solutions

Bibliography

Clouds streets and comma clouds near svalbard. https://earthobservatory.nasa.gov/images/87749/clouds-streets-and-comma-clouds-near-svalbard.

H. Affan and R. Friedrich. Spiral defect chaos in an advection-reaction-diffusion system. *Physical Review E*, 89(6):062920, June 2014. ISSN 1539-3755, 1550-2376. doi: 10.1103/PhysRevE.89.062920. URL https://link.aps.org/doi/10.1103/PhysRevE.89.062920.

Guenter Ahlers. Experiments on spatio-temporal chaos.

Mitsunobu Akiyama, Guang-Jyh Hwang, and KC Cheng. Experiments on the onset of longitudinal vortices in laminar forced convection between horizontal plates. 1971. ISSN 0022-1481.

Kerstin Avila, David Moxey, Alberto De Lozar, Marc Avila, Dwight Barkley, and Björn Hof. The Onset of Turbulence in Pipe Flow. *Science*, 333(6039):192–196, July 2011. ISSN 0036-8075, 1095-9203. doi: 10.1126/science.1203223. URL https://www.science.org/doi/10.1126/science.1203223.

Marc Avila, Ashley P. Willis, and Björn Hof. On the transient nature of localized pipe flow turbulence. *Journal of Fluid Mechanics*, 646:127–136, March 2010. ISSN 0022-1120, 1469-7645. doi: 10.1017/S0022112009993296. URL https://www.cambridge.org/core/product/identifier/S0022112009993296/type/journal_article.

Marc Avila, Dwight Barkley, and Björn Hof. Transition to Turbulence in Pipe Flow. *Annual Review of Fluid Mechanics*, 55(1):575–602, January 2023. ISSN 0066-4189, 1545-4479. doi: 10.1146/annurev-fluid-120720-025957. URL https://www.annualreviews.org/doi/10.1146/annurev-fluid-120720-025957.

Kapil M. S. Bajaj, David S. Cannell, and Guenter Ahlers. Competition between spiral-defect chaos and rolls in Rayleigh-Bénard convection. *Physical Review E*, 55(5):R4869–R4872, May 1997. ISSN 1063-651X, 1095-3787. doi: 10.1103/PhysRevE.55.R4869. URL https://link.aps.org/doi/10.1103/PhysRevE.55.R4869.

Dwight Barkley and Laurette S. Tuckerman. Computational Study of Turbulent Laminar Patterns in Couette Flow. *Physical Review Letters*, 94(1):014502, January 2005. doi: 10.1103/PhysRevLett.94.014502. URL https://link.aps.org/doi/10.1103/PhysRevLett.94.014502. Publisher: American Physical Society.

Dwight Barkley and Laurette S Tuckerman. Mean flow of turbulent–laminar patterns in plane Couette flow. *Journal of Fluid Mechanics*, 576:109–137, 2007. ISSN 1469-7645. Publisher: Cambridge University Press.

Myron J. Block. Surface Tension as the Cause of Bénard Cells and Surface Deformation in a Liquid Film. *Nature*, 178(4534):650–651, September 1956. ISSN 0028-0836, 1476-4687. doi: 10.1038/178650a0. URL https://www.nature.com/articles/178650a0.

Eberhard Bodenschatz, David S. Cannell, John R. De Bruyn, Robert Ecke, Yu-Chou Hu, Kristina Lerman, and Guenter Ahlers. Experiments on three systems with non-variational aspects. *Physica D: Nonlinear Phenomena*, 61(1-4):77–93, December 1992. ISSN 01672789. doi: 10.1016/0167-2789(92)90150-L. URL https://linkinghub.elsevier.com/retrieve/pii/016727899290150L.

Eberhard Bodenschatz, Werner Pesch, and Guenter Ahlers. Recent Developments in Rayleigh-Bénard Convection. *Annual Review of Fluid Mechanics*, 32(1):709–778, January 2000. ISSN 0066-4189, 1545-4479. doi: 10.1146/annurev.fluid.32.1.709. URL https://www.annualreviews.org/doi/10.1146/annurev.fluid.32.1.709.

Katarzyna Borońska and Laurette S. Tuckerman. Extreme multiplicity in cylindrical Rayleigh-Bénard convection. I. Time dependence and oscillations. *Physical Review E*, 81(3):036320, March 2010a. ISSN 1539-3755, 1550-2376. doi: 10.1103/PhysRevE.81.036320. URL https://link.aps.org/doi/10.1103/PhysRevE.81.036320.

Katarzyna Borońska and Laurette S. Tuckerman. Extreme multiplicity in cylindrical Rayleigh-Bénard convection. II. Bifurcation diagram and symmetry classification. *Physical Review E*, 81(3):036321, March 2010b. ISSN 1539-3755, 1550-2376. doi: 10.1103/PhysRevE.81.036321. URL https://link.aps.org/doi/10.1103/PhysRevE.81.036321.

N. Boullé, V. Dallas, and P. E. Farrell. Bifurcation analysis of two-dimensional Rayleigh-Bénard convection using deflation. *Physical Review E*, 105(5):055106, May 2022. ISSN 2470-0045, 2470-0053. doi: 10.1103/PhysRevE.105.055106. URL https://link.aps.org/doi/10.1103/PhysRevE.105.055106.

Luca Brandt. The lift-up effect: The linear mechanism behind transition and turbulence in shear flows. *European Journal of Mechanics - B/Fluids*, 47:80–96, September 2014. ISSN 09977546. doi: 10.1016/j.euromechflu.2014.03.005. URL https://linkinghub.elsevier.com/retrieve/pii/S0997754614000405.

F. H. Busse. The oscillatory instability of convection rolls in a low Prandtl number fluid. *Journal of Fluid Mechanics*, 52(1):97–112, March 1972. ISSN 0022-1120, 1469-7645. doi: 10.1017/S0022112072002988. URL https://www.cambridge.org/core/product/identifier/S0022112072002988/type/journal_article.

F H Busse. Non-linear properties of thermal convection. *Reports on Progress in Physics*, 41(12): 1929–1967, December 1978. ISSN 0034-4885, 1361-6633. doi: 10.1088/0034-4885/41/12/003. URL https://iopscience.iop.org/article/10.1088/0034-4885/41/12/003.

F. H. Busse and J. A. Whitehead. Instabilities of convection rolls in a high Prandtl number fluid. *Journal of Fluid Mechanics*, 47(2):305–320, May 1971. ISSN 0022-1120, 1469-7645. doi: 10.1017/S0022112071001071. URL https://www.cambridge.org/core/product/identifier/S0022112071001071/type/journal_article.

Kathryn M. Butler and Brian F. Farrell. Three-dimensional optimal perturbations in viscous shear flow. *Physics of Fluids A: Fluid Dynamics*, 4(8):1637–1650, August 1992. ISSN 0899-8213. doi: 10.1063/1.858386. URL https://pubs.aip.org/pof/article/4/8/1637/402702/Three-dimensional-optimal-perturbations-in-viscous.

Henri Bénard. Les tourbillons cellulaires dans une nappe liquide. - Méthodes optiques d'observation et d'enregistrement. *Journal de Physique Théorique et Appliquée*, 10(1):254–266, 1901. ISSN 0368-3893. doi: 10.1051/jphystap:0190100100025400. URL http://www.edpsciences.org/10.1051/jphystap:0190100100025400.

Reha V. Cakmur, David A. Egolf, Brendan B. Plapp, and Eberhard Bodenschatz. Bistability and Competition of Spatiotemporal Chaotic and Fixed Point Attractors in Rayleigh-Bénard Convection. *Physical Review Letters*, 79(10):1853–1856, September 1997a. ISSN 0031-9007, 1079-7114. doi: 10.1103/PhysRevLett.79.1853. URL https://link.aps.org/doi/10.1103/PhysRevLett.79.1853.

Reha V. Cakmur, David A. Egolf, Brendan B. Plapp, and Eberhard Bodenschatz. Transition from Spatiotemporal Chaos to Ideal Straight Rolls in Rayleigh-Benard Convection, February 1997b. URL http://arxiv.org/abs/patt-sol/9702003. arXiv:patt-sol/9702003.

Philippe Carrière and Peter A. Monkewitz. Convective versus absolute instability in mixed Rayleigh–Bénard–Poiseuille convection. *Journal of Fluid Mechanics*, 384:243–262, April 1999. ISSN 0022-1120, 1469-7645. doi: 10.1017/S0022112098004145. URL https://www.cambridge.org/core/product/identifier/S0022112098004145/type/journal_article.

K.-H. Chiam, M. R. Paul, M. C. Cross, and H. S. Greenside. Mean flow and spiral defect chaos in Rayleigh-Bénard convection. *Physical Review E*, 67(5):056206, May 2003. ISSN 1063-651X, 1095-3787. doi: 10.1103/PhysRevE.67.056206. URL https://link.aps.org/doi/10.1103/PhysRevE.67.056206.

R. M. Clever and F. H. Busse. Instabilities of longitudinal rolls in the presence of Poiseuille flow. *Journal of Fluid Mechanics*, 229(-1):517, August 1991. ISSN 0022-1120, 1469-7645. doi: 10.1017/S0022112091003142. URL http://www.journals.cambridge.org/abstract_S0022112091003142.

A. Cloot and G. Lebon. A nonlinear stability analysis of the Bénard–Marangoni problem. *Journal of Fluid Mechanics*, 145(-1):447, August 1984. ISSN 0022-1120, 1469-7645. doi: 10.1017/S0022112084003013. URL http://www.journals.cambridge.org/abstract_S0022112084003013.

Vincent Croquette. Convective pattern dynamics at low Prandtl number: Part I. *Contemporary Physics*, 30(2):113–133, March 1989a. ISSN 0010-7514, 1366-5812. doi: 10.1080/00107518908225511. URL http://www.tandfonline.com/doi/abs/10.1080/00107518908225511.

Vincent Croquette. Convective pattern dynamics at low Prandtl number: Part II. *Contemporary Physics*, 30(3):153–171, May 1989b. ISSN 0010-7514, 1366-5812. doi: 10.1080/00107518908222594. URL http://www.tandfonline.com/doi/abs/10.1080/00107518908222594.

W. Decker, W. Pesch, and A. Weber. Spiral defect chaos in Rayleigh-Bénard convection. *Physical Review Letters*, 73(5):648–651, August 1994. ISSN 0031-9007. doi: 10.1103/PhysRevLett.73.648. URL https://link.aps.org/doi/10.1103/PhysRevLett.73.648.

Lifang Dong, Fucheng Liu, Shuhua Liu, Yafeng He, and Weili Fan. Observation of spiral pattern and spiral defect chaos in dielectric barrier discharge in argon/air at atmospheric pressure. *Physical Review E*, 72(4):046215, October 2005. ISSN 1539-3755, 1550-2376. doi: 10.1103/PhysRevE.72.046215. URL https://link.aps.org/doi/10.1103/PhysRevE.72.046215.

Y. Duguet, P. Schlatter, and D. S. Henningson. Formation of turbulent patterns near the onset of transition in plane Couette flow. *Journal of Fluid Mechanics*, 650:119–129, May 2010. ISSN 0022-1120, 1469-7645. doi: 10.1017/S0022112010000297. URL https://www.cambridge.org/core/product/identifier/S0022112010000297/type/journal_article.

Robert E. Ecke, Yuchou Hu, Ronnie Mainieri, and Guenter Ahlers. Excitation of Spirals and Chiral Symmetry Breaking in Rayleigh-Bénard Convection. *Science*, 269(5231):1704–1707, September 1995. ISSN 0036-8075, 1095-9203. doi: 10.1126/science.269.5231.1704. URL https://www.science.org/doi/10.1126/science.269.5231.1704.

Wiktor Eckhaus. *Studies in Non-Linear Stability Theory*, volume 6 of *Springer Tracts in Natural Philosophy*. Springer Berlin Heidelberg, Berlin, Heidelberg, 1965. ISBN 978-3-642-88319-4 978-3-642-88317-0. doi: 10.1007/978-3-642-88317-0. URL http://link.springer.com/10.1007/978-3-642-88317-0.

David A. Egolf, Ilarion V. Melnikov, and Eberhard Bodenschatz. Importance of Local Pattern Properties in Spiral Defect Chaos. *Physical Review Letters*, 80(15):3228–3231, April 1998. ISSN 0031-9007, 1079-7114. doi: 10.1103/PhysRevLett.80.3228. URL https://link.aps.org/doi/10.1103/PhysRevLett.80.3228.

David A. Egolf, Ilarion V. Melnikov, Werner Pesch, and Robert E. Ecke. Mechanisms of extensive spatiotemporal chaos in Rayleigh–Bénard convection. *Nature*, 404(6779):733–736, April 2000. ISSN

0028-0836, 1476-4687. doi: 10.1038/35008013. URL https://www.nature.com/articles/35008013.

T. Ellingsen and E. Palm. Stability of linear flow. *The Physics of Fluids*, 18(4):487–488, April 1975. ISSN 0031-9171. doi: 10.1063/1.861156. URL https://pubs.aip.org/pfl/article/18/4/487/459138/Stability-of-linear-flow.

Greg Evans and Ralph Greif. Unsteady three-dimensional mixed convection in a heated horizontal channel with applications to chemical vapor deposition. *International Journal of Heat and Mass Transfer*, 34(8):2039–2051, August 1991. ISSN 00179310. doi: 10.1016/0017-9310(91)90215-Z. URL https://linkinghub.elsevier.com/retrieve/pii/001793109190215Z.

Brian F. Farrell. Optimal excitation of perturbations in viscous shear flow. *The Physics of Fluids*, 31(8):2093–2102, August 1988. ISSN 0031-9171. doi: 10.1063/1.866609. URL https://pubs.aip.org/pfl/article/31/8/2093/966463/Optimal-excitation-of-perturbations-in-viscous.

Keisuke Fukui, Masamoto Nakajima, and Hiromasa Ueda. The longitudinal vortex and its effects on the transport processes in combined free and forced laminar convection between horizontal and inclined parallel plates. *International Journal of Heat and Mass Transfer*, 26(1):109–120, January 1983. ISSN 00179310. doi: 10.1016/S0017-9310(83)80013-1. URL https://linkinghub.elsevier.com/retrieve/pii/S0017931083800131.

K. S. Gage and W. H. Reid. The stability of thermally stratified plane Poiseuille flow. *Journal of Fluid Mechanics*, 33(1):21–32, July 1968. ISSN 0022-1120, 1469-7645. doi: 10.1017/S0022112068002326. URL https://www.cambridge.org/core/product/identifier/S0022112068002326/type/journal_article.

J. F. Gibson, J. Halcrow, and P. Cvitanović. Visualizing the geometry of state space in plane Couette flow. *Journal of Fluid Mechanics*, 611:107–130, September 2008. ISSN 0022-1120, 1469-7645. doi: 10.1017/S002211200800267X. URL https://www.cambridge.org/core/product/identifier/S002211200800267X/type/journal_article.

J. F. Gibson, J. Halcrow, and P. Cvitanović. Equilibrium and travelling-wave solutions of plane Couette flow. *Journal of Fluid Mechanics*, 638:243–266, November 2009. ISSN 0022-1120, 1469-7645. doi: 10.1017/S0022112009990863. URL https://www.cambridge.org/core/product/identifier/S0022112009990863/type/journal_article.

Sébastien Gomé, Laurette S. Tuckerman, and Dwight Barkley. Statistical transition to turbulence in plane channel flow. *Physical Review Fluids*, 5(8):083905, August 2020. ISSN 2469-990X. doi: 10.1103/PhysRevFluids.5.083905. URL https://link.aps.org/doi/10.1103/PhysRevFluids.5.083905.

Michael D. Graham and Daniel Floryan. Exact Coherent States and the Nonlinear Dynamics of Wall-Bounded Turbulent Flows. *Annual Review of Fluid Mechanics*, 53(1):227–253, January

2021. ISSN 0066-4189, 1545-4479. doi: 10.1146/annurev-fluid-051820-020223. URL https://www.annualreviews.org/doi/10.1146/annurev-fluid-051820-020223.

J. Halcrow, J. F. Gibson, P. Cvitanović, and D. Viswanath. Heteroclinic connections in plane Couette flow. *Journal of Fluid Mechanics*, 621:365–376, February 2009. ISSN 0022-1120, 1469-7645. doi: 10.1017/S0022112008005065. URL https://www.cambridge.org/core/product/identifier/S0022112008005065/type/journal_article.

James M. Hamilton, John Kim, and Fabian Waleffe. Regeneration mechanisms of near-wall turbulence structures. *Journal of Fluid Mechanics*, 287:317–348, March 1995. ISSN 0022-1120, 1469-7645. doi: 10.1017/S0022112095000978. URL https://www.cambridge.org/core/product/identifier/S0022112095000978/type/journal_article.

C.Q Hoard, C.R Robertson, and A Acrivos. Experiments on the cellular structure in bénard convection. *International Journal of Heat and Mass Transfer*, 13(5):849–856, May 1970. ISSN 00179310. doi: 10.1016/0017-9310(70)90130-4. URL https://linkinghub.elsevier.com/retrieve/pii/0017931070901304.

B. Hof, P. G. J. Lucas, and T. Mullin. Flow state multiplicity in convection. *Physics of Fluids*, 11(10):2815–2817, October 1999. ISSN 1070-6631, 1089-7666. doi: 10.1063/1.870178. URL https://pubs.aip.org/pof/article/11/10/2815/254396/Flow-state-multiplicity-in-convection.

M. Z. Hossain and J. M. Floryan. Drag reduction in a thermally modulated channel. *Journal of Fluid Mechanics*, 791:122–153, March 2016. ISSN 0022-1120, 1469-7645. doi: 10.1017/jfm.2016.42. URL https://www.cambridge.org/core/product/identifier/S0022112016000422/type/journal_article.

M. Z. Hossain and J. M. Floryan. On the role of surface grooves in the reduction of pressure losses in heated channels. *Physics of Fluids*, 32(8):083610, August 2020. ISSN 1070-6631, 1089-7666. doi: 10.1063/5.0018416. URL https://pubs.aip.org/pof/article/32/8/083610/1060903/On-the-role-of-surface-grooves-in-the-reduction-of.

M. Z. Hossain, D. Floryan, and J. M. Floryan. Drag reduction due to spatial thermal modulations. *Journal of Fluid Mechanics*, 713:398–419, December 2012. ISSN 0022-1120, 1469-7645. doi: 10.1017/jfm.2012.465. URL https://www.cambridge.org/core/product/identifier/S002211201200465X/type/journal_article.

Yuchou Hu, Robert Ecke, and Guenter Ahlers. Convection near threshold for Prandtl numbers near 1. *Physical Review E*, 48(6):4399–4413, December 1993. ISSN 1063-651X, 1095-3787. doi: 10.1103/PhysRevE.48.4399. URL https://link.aps.org/doi/10.1103/PhysRevE.48.4399.

Yuchou Hu, Robert Ecke, and Guenter Ahlers. Convection for Prandtl numbers near 1: Dynamics of textured patterns. *Physical Review E*, 51(4):3263–3279, April 1995. ISSN 1063-651X, 1095-3787.

doi: 10.1103/PhysRevE.51.3263. URL https://link.aps.org/doi/10.1103/PhysRevE.51.3263.

Yuchou Hu, Robert E. Ecke, and Guenter Ahlers. Convection under rotation for Prandtl numbers near 1: Linear stability, wave-number selection, and pattern dynamics. *Physical Review E*, 55(6): 6928–6949, June 1997. ISSN 1063-651X, 1095-3787. doi: 10.1103/PhysRevE.55.6928. URL https://link.aps.org/doi/10.1103/PhysRevE.55.6928.

Harold Jeffreys. Some cases of instability in fluid motion. *Proceedings of the Royal Society of London. Series A, Containing Papers of a Mathematical and Physical Character*, 118(779):195–208, March 1928. ISSN 0950-1207, 2053-9150. doi: 10.1098/rspa.1928.0045. URL https://royalsocietypublishing.org/doi/10.1098/rspa.1928.0045.

Klavs F. Jensen, Erik O. Einset, and Dimitrios I. Fotiadis. Flow Phenomena in Chemical Vapor Deposition of Thin Films. *Annual Review of Fluid Mechanics*, 23(1):197–232, January 1991. ISSN 0066-4189, 1545-4479. doi: 10.1146/annurev.fl.23.010191.001213. URL https://www.annualreviews.org/doi/10.1146/annurev.fl.23.010191.001213.

J. John Soundar Jerome, Jean-Marc Chomaz, and Patrick Huerre. Transient growth in Rayleigh-Bénard-Poiseuille/Couette convection. *Physics of Fluids*, 24(4):044103, April 2012. ISSN 1070-6631, 1089-7666. doi: 10.1063/1.4704642. URL https://pubs.aip.org/pof/article/24/4/044103/257562/Transient-growth-in-Rayleigh-Benard-Poiseuille.

A. Karimi, Zhi-Feng Huang, and M. R. Paul. Exploring spiral defect chaos in generalized Swift-Hohenberg models with mean flow. *Physical Review E*, 84(4):046215, October 2011. ISSN 1539-3755, 1550-2376. doi: 10.1103/PhysRevE.84.046215. URL https://link.aps.org/doi/10.1103/PhysRevE.84.046215.

George Karniadakis and Spencer J Sherwin. *Spectral/hp element methods for computational fluid dynamics*. Oxford University Press, 2005. ISBN 0-19-852869-8.

Genta Kawahara and Shigeo Kida. Periodic motion embedded in plane Couette turbulence: regeneration cycle and burst. *Journal of Fluid Mechanics*, 449:291–300, December 2001. ISSN 0022-1120, 1469-7645. doi: 10.1017/S0022112001006243. URL https://www.cambridge.org/core/product/identifier/S0022112001006243/type/journal_article.

R.E. Kelly. The Onset and Development of Thermal Convection in Fully Developed Shear Flows. In *Advances in Applied Mechanics*, volume 31, pages 35–112. Elsevier, 1994. ISBN 978-0-12-002031-7. doi: 10.1016/S0065-2156(08)70255-2. URL https://linkinghub.elsevier.com/retrieve/pii/S0065215608702552.

K.J. Kennedy and A. Zebib. Combined free and forced convection between horizontal parallel planes: some case studies. *International Journal of Heat and Mass Transfer*, 26(3):471–474, March 1983. ISSN 00179310. doi: 10.1016/0017-9310(83)90052-2. URL https://linkinghub.elsevier.com/retrieve/pii/0017931083900522.

E.L. Koschmieder and S.G. Pallas. Heat transfer through a shallow, horizontal convecting fluid layer. *International Journal of Heat and Mass Transfer*, 17(9):991–1002, September 1974. ISSN 00179310. doi: 10.1016/0017-9310(74)90181-1. URL https://linkinghub.elsevier.com/retrieve/pii/0017931074901811.

P. Le Gal, A. Pocheau, and V. Croquette. Square versus Roll Pattern at Convective Threshold. *Physical Review Letters*, 54(23):2501–2504, June 1985. ISSN 0031-9007. doi: 10.1103/PhysRevLett.54.2501. URL https://link.aps.org/doi/10.1103/PhysRevLett.54.2501.

Jun Liu and Guenter Ahlers. Spiral-Defect Chaos in Rayleigh-Bénard Convection with Small Prandtl Numbers. *P H Y S I C A L R E V I E W L E T T E R S*, 77(15), 1996.

Mary Lowe and J. P. Gollub. Pattern Selection near the Onset of Convection: The Eckhaus Instability. *Physical Review Letters*, 55(23):2575–2578, December 1985. ISSN 0031-9007. doi: 10.1103/PhysRevLett.55.2575. URL https://link.aps.org/doi/10.1103/PhysRevLett.55.2575.

J-M Luijkx, Jean Karl Platten, and J Cl Legros. On the existence of thermoconvective rolls, transverse to a superimposed mean Poiseuille flow. *International Journal of Heat and Mass Transfer*, 24(7):1287–1291, 1981. ISSN 0017-9310. Publisher: Elsevier.

Dong-Jun Ma, De-Jun Sun, and Xie-Yuan Yin. Multiplicity of steady states in cylindrical Rayleigh-Bénard convection. *Physical Review E*, 74(3):037302, September 2006. ISSN 1539-3755, 1550-2376. doi: 10.1103/PhysRevE.74.037302. URL https://link.aps.org/doi/10.1103/PhysRevE.74.037302.

Paul Manneville. Rayleigh-Bénard Convection: Thirty Years of Experimental, Theoretical, and Modeling Work. In Gerhard Höhler, Johann H. Kühn, Thomas Müller, Joachim Trümper, Andrei Ruckenstein, Peter Wölfle, Frank Steiner, Innocent Mutabazi, José Eduardo Wesfreid, and Etienne Guyon, editors, *Dynamics of Spatio-Temporal Cellular Structures*, volume 207, pages 41–65. Springer New York, New York, NY, 2006. ISBN 978-0-387-40098-3 978-0-387-25111-0. doi: 10.1007/978-0-387-25111-0_3. URL http://link.springer.com/10.1007/978-0-387-25111-0_3. Series Title: Springer Tracts in Modern Physics.

Á. Meseguer and L.N. Trefethen. Linearized pipe flow to Reynolds number 107. *Journal of Computational Physics*, 186(1):178–197, March 2003. ISSN 00219991. doi: 10.1016/S0021-9991(03)00029-9. URL https://linkinghub.elsevier.com/retrieve/pii/S0021999103000299.

Stephen W. Morris, Eberhard Bodenschatz, David S. Cannell, and Guenter Ahlers. Spiral defect chaos in large aspect ratio Rayleigh-Bénard convection. *Physical Review Letters*, 71(13):2026–2029, September 1993. ISSN 0031-9007. doi: 10.1103/PhysRevLett.71.2026. URL https://link.aps.org/doi/10.1103/PhysRevLett.71.2026.

Stephen W. Morris, Eberhard Bodenschatz, David S. Cannell, and Guenter Ahlers. The spatio-temporal structure of spiral-defect chaos. *Physica D: Nonlinear Phenomena*, 97(1-3):164–179, October 1996.

ISSN 01672789. doi: 10.1016/0167-2789(96)00096-6. URL https://linkinghub.elsevier.com/retrieve/pii/0167278996000966.

H. W. Müller, M. Lücke, and M. Kamps. Transversal convection patterns in horizontal shear flow. *Physical Review A*, 45(6):3714–3726, March 1992. ISSN 1050-2947, 1094-1622. doi: 10.1103/PhysRevA.45.3714. URL https://link.aps.org/doi/10.1103/PhysRevA.45.3714.

M. Nagata. Three-dimensional finite-amplitude solutions in plane Couette flow: bifurcation from infinity. *Journal of Fluid Mechanics*, 217:519–527, August 1990. ISSN 0022-1120, 1469-7645. doi: 10.1017/S0022112090000829. URL https://www.cambridge.org/core/product/identifier/S0022112090000829/type/journal_article.

M. Nagata. Three-dimensional traveling-wave solutions in plane Couette flow. *Physical Review E*, 55 (2):2023–2025, February 1997. ISSN 1063-651X, 1095-3787. doi: 10.1103/PhysRevE.55.2023. URL https://link.aps.org/doi/10.1103/PhysRevE.55.2023.

X. Nicolas, A. Mojtabi, and J. K. Platten. Two-dimensional numerical analysis of the Poiseuille–Bénard flow in a rectangular channel heated from below. *Physics of Fluids*, 9(2):337–348, February 1997. ISSN 1070-6631, 1089-7666. doi: 10.1063/1.869235. URL https://pubs.aip.org/pof/article/9/2/337/259822/Two-dimensional-numerical-analysis-of-the.

X. Nicolas, J.-M. Luijkx, and J.-K. Platten. Linear stability of mixed convection flows in horizontal rectangular channels of finite transversal extension heated from below. *International Journal of Heat and Mass Transfer*, 43(4):589–610, February 2000. ISSN 00179310. doi: 10.1016/S0017-9310(99)00099-X. URL https://linkinghub.elsevier.com/retrieve/pii/S001793109900099X.

Xavier Nicolas. Revue bibliographique sur les écoulements de Poiseuille–Rayleigh–Bénard : écoulements de convection mixte en conduites rectangulaires horizontales chauffées par le bas. *International Journal of Thermal Sciences*, 41(10):961–1016, October 2002. ISSN 12900729. doi: 10.1016/S1290-0729(02)01374-1. URL https://linkinghub.elsevier.com/retrieve/pii/S1290072902013741.

Xavier Nicolas, Shihe Xin, and Noussaiba Zoueidi. Characterisation of a Wavy Convective Instability in Poiseuille-Rayleigh-Be´nard Flows: Linear Stability Analysis and Non Linear Numerical Simulations Under Random Excitations. In *2010 14th International Heat Transfer Conference, Volume 7*, pages 203–208, Washington, DC, USA, January 2010. ASMEDC. ISBN 978-0-7918-4942-2 978-0-7918-3879-2. doi: 10.1115/IHTC14-22256. URL https://asmedigitalcollection.asme.org/IHTC/proceedings/IHTC14/49422/203/360332.

Xavier Nicolas, Noussaiba Zoueidi, and Shihe Xin. Influence of a white noise at channel inlet on the parallel and wavy convective instabilities of Poiseuille-Rayleigh-Bénard flows. *Physics of Fluids*, 24(8):084101, August 2012. ISSN 1070-6631, 1089-7666. doi: 10.1063/1.4737652. URL https://pubs.aip.org/pof/article/24/8/084101/258132/Influence-of-a-white-noise-at-channel-inlet-on-the.

William M'F. Orr. The Stability or Instability of the Steady Motions of a Perfect Liquid and of a Viscous Liquid. Part II: A Viscous Liquid. *Proceedings of the Royal Irish Academy. Section A: Mathematical and Physical Sciences*, 27:69–138, 1907. ISSN 00358975. URL http://www.jstor.org/stable/20490591. Publisher: Royal Irish Academy.

Steven A. Orszag. Accurate solution of the Orr–Sommerfeld stability equation. *Journal of Fluid Mechanics*, 50(4):689–703, December 1971. ISSN 0022-1120, 1469-7645. doi: 10.1017/S0022112071002842. URL https://www.cambridge.org/core/product/identifier/S0022112071002842/type/journal_article.

S. Ostrach and Y. Kamotani. Heat Transfer Augmentation in Laminar Fully Developed Channel Flow by Means of Heating From Below. *Journal of Heat Transfer*, 97(2):220–225, May 1975. ISSN 0022-1481, 1528-8943. doi: 10.1115/1.3450344. URL https://asmedigitalcollection.asme.org/heattransfer/article/97/2/220/416581/Heat-Transfer-Augmentation-in-Laminar-Fully.

MT Ouazzani, Jean-Paul Caltagirone, Gilles Meyer, and Abdelkader Mojtabi. Etude numerique et expérimentale de la convection mixte entre deux plans horizontaux à températures différentes. *International journal of heat and mass transfer*, 32(2):261–269, 1989. ISSN 0017-9310. Publisher: Elsevier.

MT Ouazzani, Jean Karl Platten, and Abdelkader Mojtabi. Etude expérimentale de la convection mixte entre deux plans horizontaux à températures différentes—II. *International journal of heat and mass transfer*, 33(7):1417–1427, 1990. ISSN 0017-9310. Publisher: Elsevier.

Hervé Pabiou, Xavier Nicolas, Shihe Xin, and Sophie Mergui. Observations d'une instabilité convective apparaissant sous la forme de rouleaux sinueux dans un écoulement de Poiseuille–Rayleigh–Bénard. *Mécanique & industries*, 4(5):537–543, 2003. ISSN 1296-2139. Publisher: Elsevier.

Hervé Pabiou, Sophie Mergui, and Christine Bénard. Wavy secondary instability of longitudinal rolls in RayleighPoiseuille flows. *Journal of Fluid Mechanics*, 542(-1):175, October 2005. ISSN 0022-1120, 1469-7645. doi: 10.1017/S0022112005006154. URL http://www.journals.cambridge.org/abstract_S0022112005006154.

Chaitanya S Paranjape. Onset of turbulence in plane Poiseuille flow. 2019. Publisher: IST Austria Klosterneuburg, Austria.

Chaitanya S. Paranjape, Yohann Duguet, and Björn Hof. Oblique stripe solutions of channel flow. *Journal of Fluid Mechanics*, 897:A7, August 2020. ISSN 0022-1120, 1469-7645. doi: 10.1017/jfm.2020.322. URL https://www.cambridge.org/core/product/identifier/S0022112020003225/type/journal_article.

Chaitanya S. Paranjape, Gökhan Yalnız, Yohann Duguet, Nazmi Burak Budanur, and Björn Hof. Direct Path from Turbulence to Time-Periodic Solutions. *Physical Review Letters*, 131(3):034002,

July 2023. ISSN 0031-9007, 1079-7114. doi: 10.1103/PhysRevLett.131.034002. URL https://link.aps.org/doi/10.1103/PhysRevLett.131.034002.

M. R. Paul, M. I. Einarsson, P. F. Fischer, and M. C. Cross. Extensive chaos in Rayleigh-Bénard convection. *Physical Review E*, 75(4):045203, April 2007. ISSN 1539-3755, 1550-2376. doi: 10.1103/PhysRevE.75.045203. URL https://link.aps.org/doi/10.1103/PhysRevE.75.045203.

M.R. Paul, K.-H. Chiam, M.C. Cross, P.F. Fischer, and H.S. Greenside. Pattern formation and dynamics in Rayleigh–Bénard convection: numerical simulations of experimentally realistic geometries. *Physica D: Nonlinear Phenomena*, 184(1-4):114–126, October 2003. ISSN 01672789. doi: 10.1016/S0167-2789(03)00216-1. URL https://linkinghub.elsevier.com/retrieve/pii/S0167278903002161.

Anne Pellew and Richard Vynne Southwell. On maintained convective motion in a fluid heated from below. *Proceedings of the Royal Society of London. Series A. Mathematical and Physical Sciences*, 176(966):312–343, November 1940. ISSN 0080-4630, 2053-9169. doi: 10.1098/rspa.1940.0092. URL https://royalsocietypublishing.org/doi/10.1098/rspa.1940.0092.

Sergio Pirozzoli, Matteo Bernardini, Roberto Verzicco, and Paolo Orlandi. Mixed convection in turbulent channels with unstable stratification. *Journal of Fluid Mechanics*, 821:482–516, June 2017. ISSN 0022-1120, 1469-7645. doi: 10.1017/jfm.2017.216. URL https://www.cambridge.org/core/product/identifier/S0022112017002166/type/journal_article.

Brendan B Plapp and Eberhard Bodenschatz. Core dynamics of multi-armed spirals in Rayleigh-Bénard convection. *Physica Scripta*, T67:111–116, January 1996. ISSN 0031-8949, 1402-4896. doi: 10.1088/0031-8949/1996/T67/022. URL https://iopscience.iop.org/article/10.1088/0031-8949/1996/T67/022.

Brendan B. Plapp, David A. Egolf, Eberhard Bodenschatz, and Werner Pesch. Dynamics and Selection of Giant Spirals in Rayleigh-Bénard Convection. *Physical Review Letters*, 81(24):5334–5337, December 1998. ISSN 0031-9007, 1079-7114. doi: 10.1103/PhysRevLett.81.5334. URL https://link.aps.org/doi/10.1103/PhysRevLett.81.5334.

Brendan Bryce Plapp. Spiral pattern formation in Rayleigh-Benard convection. *Ph.D. Thesis*, page 3118, December 1997. URL https://ui.adsabs.harvard.edu/abs/1997PhDT.....105P.

A. Prigent and O. Dauchot. "Barber pole turbulence" in large aspect ratio Taylor-Couette flow. *Physical Review Letters*, 89(1):014501, June 2002. ISSN 0031-9007, 1079-7114. doi: 10.1103/PhysRevLett.89.014501. URL http://arxiv.org/abs/cond-mat/0009241. arXiv:cond-mat/0009241.

Arnaud Prigent, Guillaume Grégoire, Hugues Chaté, and Olivier Dauchot. Long-wavelength modulation of turbulent shear flows. *Physica D: Nonlinear Phenomena*, 174(1-4):100–113, January 2003. ISSN 01672789. doi: 10.1016/S0167-2789(02)00685-1. URL https://linkinghub.elsevier.com/retrieve/pii/S0167278902006851.

Subhashis Ray and J. Srinivasan. Analysis of conjugate laminar mixed convection cooling in a shrouded array of electronic components. *International Journal of Heat and Mass Transfer*, 35 (4):815–822, April 1992. ISSN 00179310. doi: 10.1016/0017-9310(92)90249-R. URL https://linkinghub.elsevier.com/retrieve/pii/001793109290249R.

Lord Rayleigh. LIX. *On convection currents in a horizontal layer of fluid, when the higher temperature is on the under side*. *The London, Edinburgh, and Dublin Philosophical Magazine and Journal of Science*, 32(192):529–546, December 1916. ISSN 1941-5982, 1941-5990. doi: 10.1080/14786441608635602. URL https://www.tandfonline.com/doi/full/10.1080/14786441608635602.

Satish C. Reddy and Dan S. Henningson. Energy growth in viscous channel flows. *Journal of Fluid Mechanics*, 252:209–238, July 1993. ISSN 0022-1120, 1469-7645. doi: 10.1017/S0022112093003738. URL https://www.cambridge.org/core/product/identifier/S0022112093003738/type/journal_article.

Satish C. Reddy, Peter J. Schmid, and Dan S. Henningson. Pseudospectra of the Orr–Sommerfeld Operator. *SIAM Journal on Applied Mathematics*, 53(1):15–47, February 1993. ISSN 0036-1399, 1095-712X. doi: 10.1137/0153002. URL http://epubs.siam.org/doi/10.1137/0153002.

Florian Reetz and Tobias M. Schneider. Invariant states in inclined layer convection. Part 1. Temporal transitions along dynamical connections between invariant states. *Journal of Fluid Mechanics*, 898:A22, September 2020. ISSN 0022-1120, 1469-7645. doi: 10.1017/jfm.2020.317. URL https://www.cambridge.org/core/product/identifier/S0022112020003171/type/journal_article.

Florian Reetz, Tobias Kreilos, and Tobias M. Schneider. Exact invariant solution reveals the origin of self-organized oblique turbulent-laminar stripes. *Nature Communications*, 10(1):2277, May 2019. ISSN 2041-1723. doi: 10.1038/s41467-019-10208-x. URL https://doi.org/10.1038/s41467-019-10208-x.

Florian Reetz, Priya Subramanian, and Tobias M. Schneider. Invariant states in inclined layer convection. Part 2. Bifurcations and connections between branches of invariant states. *Journal of Fluid Mechanics*, 898:A23, September 2020. ISSN 0022-1120, 1469-7645. doi: 10.1017/jfm.2020.318. URL https://www.cambridge.org/core/product/identifier/S0022112020003183/type/journal_article.

Osborne Reynolds. XXIX. An experimental investigation of the circumstances which determine whether the motion of water shall be direct or sinuous, and of the law of resistance in parallel channels. *Philosophical Transactions of the Royal Society of London*, 174:935–982, December 1883. ISSN 0261-0523, 2053-9223. doi: 10.1098/rstl.1883.0029. URL https://royalsocietypublishing.org/doi/10.1098/rstl.1883.0029.

Osborne Reynolds. IV. On the dynamical theory of incompressible viscous fluids and the determination of the criterion. *Philosophical Transactions of the Royal Society of London. (A.)*, 186:123–164,

December 1895. ISSN 0264-3820, 2053-9231. doi: 10.1098/rsta.1895.0004. URL https://royalsocietypublishing.org/doi/10.1098/rsta.1895.0004.

H. T. Rossby. A study of Bénard convection with and without rotation. *Journal of Fluid Mechanics*, 36(2):309–335, April 1969. ISSN 0022-1120, 1469-7645. doi: 10.1017/S0022112069001674. URL https://www.cambridge.org/core/product/identifier/S0022112069001674/type/journal_article.

Sten Rüdiger and Fred Feudel. Pattern formation in Rayleigh-Bénard convection in a cylindrical container. *Physical Review E*, 62(4):4927–4931, October 2000. ISSN 1063-651X, 1095-3787. doi: 10.1103/PhysRevE.62.4927. URL https://link.aps.org/doi/10.1103/PhysRevE.62.4927.

A. Scagliarini, H. Einarsson, Á. Gylfason, and F. Toschi. Law of the wall in an unstably stratified turbulent channel flow. *Journal of Fluid Mechanics*, 781:R5, October 2015. ISSN 0022-1120, 1469-7645. doi: 10.1017/jfm.2015.498. URL https://www.cambridge.org/core/product/identifier/S002211201500498X/type/journal_article.

Andrea Scagliarini, Armann Gylfason, and Federico Toschi. Heat flux scaling in turbulent Rayleigh-Bénard convection with an imposed longitudinal wind. *Physical Review E*, 89(4):043012, April 2014. ISSN 1539-3755, 1550-2376. doi: 10.1103/PhysRevE.89.043012. URL http://arxiv.org/abs/1311.4598. arXiv:1311.4598 [physics].

H. Schlichting. Zur Enstehung der Turbulenz bei der Plattenströmung. *Nachrichten von der Gesellschaft der Wissenschaften zu Göttingen, Mathematisch-Physikalische Klasse*, 1933:181–208, 1933. URL http://eudml.org/doc/59420.

Hermann Schlichting and Klaus Gersten. Onset of Turbulence (Stability Theory). In *Boundary-Layer Theory*, pages 415–496. Springer Berlin Heidelberg, Berlin, Heidelberg, 2017. ISBN 978-3-662-52917-1 978-3-662-52919-5. doi: 10.1007/978-3-662-52919-5_15. URL http://link.springer.com/10.1007/978-3-662-52919-5_15.

A. Schlüter, D. Lortz, and F. Busse. On the stability of steady finite amplitude convection. *Journal of Fluid Mechanics*, 23(01):129, September 1965. ISSN 0022-1120, 1469-7645. doi: 10.1017/S0022112065001271. URL http://www.journals.cambridge.org/abstract_S0022112065001271.

Peter J. Schmid. Nonmodal Stability Theory. *Annual Review of Fluid Mechanics*, 39(1):129–162, January 2007. ISSN 0066-4189, 1545-4479. doi: 10.1146/annurev.fluid.38.050304.092139. URL https://www.annualreviews.org/doi/10.1146/annurev.fluid.38.050304.092139.

Peter J. Schmid and Dan S. Henningson. *Stability and Transition in Shear Flows*, volume 142 of *Applied Mathematical Sciences*. Springer New York, New York, NY, 2001. ISBN 978-1-4612-6564-1 978-1-4613-0185-1. doi: 10.1007/978-1-4613-0185-1. URL http://link.springer.com/10.1007/978-1-4613-0185-1.

Rainer Schmitz, Werner Pesch, and Walter Zimmermann. Spiral-defect chaos: Swift-Hohenberg model versus Boussinesq equations. *Physical Review E*, 65(3):037302, March 2002. ISSN 1063-651X, 1095-3787. doi: 10.1103/PhysRevE.65.037302. URL https://link.aps.org/doi/10.1103/PhysRevE.65.037302.

Masaki Shimizu and Paul Manneville. Bifurcations to turbulence in transitional channel flow. *Physical Review Fluids*, 4(11):113903, November 2019. doi: 10.1103/PhysRevFluids.4.113903. URL https://link.aps.org/doi/10.1103/PhysRevFluids.4.113903. Publisher: American Physical Society.

Jennifer H. Siggers. Dynamics of target patterns in low-Prandtl-number convection. *Journal of Fluid Mechanics*, 475:357–375, January 2003. ISSN 0022-1120, 1469-7645. doi: 10.1017/S0022112002002896. URL https://www.cambridge.org/core/product/identifier/S0022112002002896/type/journal_article.

Arnold Sommerfeld. *Ein beitrag zur hydrodynamischen erklaerung der turbulenten fluessigkeitsbewegungen*. 1909.

Baofang Song, Dwight Barkley, Björn Hof, and Marc Avila. Speed and structure of turbulent fronts in pipe flow. *Journal of Fluid Mechanics*, 813:1045–1059, February 2017. ISSN 0022-1120, 1469-7645. doi: 10.1017/jfm.2017.14. URL https://www.cambridge.org/core/product/identifier/S0022112017000143/type/journal_article.

Herbert Brian Squire. On the stability for three-dimensional disturbances of viscous fluid flow between parallel walls. *Proceedings of the Royal Society of London. Series A, Containing Papers of a Mathematical and Physical Character*, 142(847):621–628, November 1933. ISSN 0950-1207, 2053-9150. doi: 10.1098/rspa.1933.0193. URL https://royalsocietypublishing.org/doi/10.1098/rspa.1933.0193.

J. Swift and P. C. Hohenberg. Hydrodynamic fluctuations at the convective instability. *Physical Review A*, 15(1):319–328, January 1977. ISSN 0556-2791. doi: 10.1103/PhysRevA.15.319. URL https://link.aps.org/doi/10.1103/PhysRevA.15.319.

J. J. Tao, Bruno Eckhardt, and X. M. Xiong. Extended localized structures and the onset of turbulence in channel flow. *Physical Review Fluids*, 3(1):011902, January 2018. doi: 10.1103/PhysRevFluids.3.011902. URL https://link.aps.org/doi/10.1103/PhysRevFluids.3.011902. Publisher: American Physical Society.

W. Tollmien. Über die Entstehung der Turbulenz. 1. Mitteilung. *Nachrichten von der Gesellschaft der Wissenschaften zu Göttingen, Mathematisch-Physikalische Klasse*, 1929:21–44, 1928. URL http://eudml.org/doc/59276.

Lloyd N. Trefethen. Pseudospectra of Linear Operators. *SIAM Review*, 39(3):383–406, January 1997. ISSN 0036-1445, 1095-7200. doi: 10.1137/S0036144595295284. URL http://epubs.siam.org/doi/10.1137/S0036144595295284.

Takahiro Tsukahara, Kaoru Iwamoto, Hiroshi Kawamura, and Tetsuaki Takeda. DNS of heat transfer in a transitional channel flow accompanied by a turbulent puff-like structure, September 2014a. URL http://arxiv.org/abs/1406.0586. arXiv:1406.0586 [physics].

Takahiro Tsukahara, Yasuo Kawaguchi, and Hiroshi Kawamura. An experimental study on turbulent-stripe structure in transitional channel flow, 2014b. URL https://arxiv.org/abs/1406.1378. Version Number: 2.

Takahiro Tsukahara, Yohji Seki, Hiroshi Kawamura, and Daisuke Tochio. DNS of turbulent channel flow at very low Reynolds numbers, September 2014c. URL http://arxiv.org/abs/1406.0248. arXiv:1406.0248 [physics].

Laurette S. Tuckerman and Dwight Barkley. Global Bifurcation to Traveling Waves in Axisymmetric Convection. *Physical Review Letters*, 61(4):408–411, July 1988. ISSN 0031-9007. doi: 10.1103/PhysRevLett.61.408. URL https://link.aps.org/doi/10.1103/PhysRevLett.61.408.

Laurette S Tuckerman and Dwight Barkley. Patterns and dynamics in transitional plane Couette flow. *Physics of Fluids*, 23(4), 2011. ISSN 1070-6631. Publisher: AIP Publishing.

Laurette S. Tuckerman, Tobias Kreilos, Hecke Schrobsdorff, Tobias M. Schneider, and John F. Gibson. Turbulent-laminar patterns in plane Poiseuille flow. *Physics of Fluids*, 26(11):114103, November 2014. ISSN 1070-6631, 1089-7666. doi: 10.1063/1.4900874. URL https://pubs.aip.org/pof/article/26/11/114103/315350/Turbulent-laminar-patterns-in-plane-Poiseuille.

Geoffrey K. Vallis, Douglas J. Parker, and Steven M. Tobias. A simple system for moist convection: the Rainy–Bénard model. *Journal of Fluid Mechanics*, 862:162–199, March 2019. ISSN 0022-1120, 1469-7645. doi: 10.1017/jfm.2018.954. URL https://www.cambridge.org/core/product/identifier/S0022112018009540/type/journal_article.

Milton Van Dyke and Milton Van Dyke. *An album of fluid motion*, volume 176. Parabolic Press Stanford, 1982.

D. Viswanath. Recurrent motions within plane Couette turbulence. *Journal of Fluid Mechanics*, 580:339–358, June 2007. ISSN 0022-1120, 1469-7645. doi: 10.1017/S0022112007005459. URL https://www.cambridge.org/core/product/identifier/S0022112007005459/type/journal_article.

Eduardo Vitral, Saikat Mukherjee, Perry H. Leo, Jorge Viñals, Mark R. Paul, and Zhi-Feng Huang. Spiral defect chaos in Rayleigh-Bénard convection: Asymptotic and numerical studies of azimuthal flows induced by rotating spirals. *Physical Review Fluids*, 5(9):093501, September 2020. ISSN 2469-990X. doi: 10.1103/PhysRevFluids.5.093501. URL https://link.aps.org/doi/10.1103/PhysRevFluids.5.093501.

Fabian Waleffe. Exact coherent structures in channel flow. *Journal of Fluid Mechanics*, 435:93–102, May 2001. ISSN 0022-1120, 1469-7645. doi: 10.1017/S0022112001004189. URL https://www.cambridge.org/core/product/identifier/S0022112001004189/type/journal_article.

Fabian Waleffe. Homotopy of exact coherent structures in plane shear flows. *Physics of Fluids*, 15(6):1517–1534, June 2003. ISSN 1070-6631, 1089-7666. doi: 10.1063/1.1566753. URL https://pubs.aip.org/pof/article/15/6/1517/448391/Homotopy-of-exact-coherent-structures-in-plane.

José Eduardo Wesfreid. Henri Bénard: Thermal convection and vortex shedding. *Comptes Rendus. Mécanique*, 345(7):446–466, June 2017. ISSN 1873-7234. doi: 10.1016/j.crme.2017.06.006. URL https://comptes-rendus.academie-sciences.fr/mecanique/articles/10.1016/j.crme.2017.06.006/.

G. E. Willis and J. W. Deardorff. The oscillatory motions of Rayleigh convection. *Journal of Fluid Mechanics*, 44(04):661, December 1970. ISSN 0022-1120, 1469-7645. doi: 10.1017/S0022112070002070. URL http://www.journals.cambridge.org/abstract_S0022112070002070.

Hao-wen Xi, J. D. Gunton, and Jorge Viñals. Spiral defect chaos in a model of Rayleigh-Bénard convection. *Physical Review Letters*, 71(13):2030–2033, September 1993. ISSN 0031-9007. doi: 10.1103/PhysRevLett.71.2030. URL https://link.aps.org/doi/10.1103/PhysRevLett.71.2030.

Haowen Xi and J. D. Gunton. Spatiotemporal chaos in a model of Rayleigh-Bénard convection. *Physical Review E*, 52(5):4963–4975, November 1995. ISSN 1063-651X, 1095-3787. doi: 10.1103/PhysRevE.52.4963. URL https://link.aps.org/doi/10.1103/PhysRevE.52.4963.

Xiangkai Xiao and Baofang Song. The growth mechanism of turbulent bands in channel flow at low Reynolds numbers. *Journal of Fluid Mechanics*, 883:R1, January 2020. ISSN 0022-1120, 1469-7645. doi: 10.1017/jfm.2019.899. URL https://www.cambridge.org/core/product/identifier/S0022112019008991/type/journal_article.

Shihe Xin, Xavier Nicolas, and Patrick Le Quéré. Stability analyses of Longitudinal Rolls of Poiseuille-Rayleigh-Bénard Flows in Air-Filled Channels of Finite Transversal Extension. *Numerical Heat Transfer, Part A: Applications*, 50(5):467–490, July 2006. ISSN 1040-7782, 1521-0634. doi: 10.1080/10407780600620079. URL http://www.tandfonline.com/doi/abs/10.1080/10407780600620079.

Xiangming Xiong, Jianjun Tao, Shiyi Chen, and Luca Brandt. Turbulent bands in plane-Poiseuille flow at moderate Reynolds numbers. *Physics of Fluids*, 27(4):041702, April 2015. ISSN 1070-6631, 1089-7666. doi: 10.1063/1.4917173. URL https://pubs.aip.org/pof/article/27/4/041702/1019208/Turbulent-bands-in-plane-Poiseuille-flow-at.